Ocean Modelling 171 (2022) 101958

Contents lists available at ScienceDirect

Ocean Modelling

journal homepage: www.elsevier.com/locate/ocemod

A new K-profile parameterization for the ocean surface boundary layer under realistic forcing conditions

Miguel Solano [a,*], Yalin Fan [b]

[a] The University of Southern Mississippi, Stennis Space Center, MS, United States of America
[b] US Naval Research Laboratory, Stennis Space Center, MS, United States of America

ARTICLE INFO

Keywords:
Langmuir turbulence
KPP
NCOM
Ocean surface boundary layer
Vertical mixing

ABSTRACT

In this study, we present a new parameterization for the enhancement of vertical mixing brought by the inclusion of the Stokes drift for the turbulent mixing schemes in ocean circulation models. The new scheme (KPP-LT) uses the K-Profile Parameterization (Large et al., 1994) as a template, and attempts to include the effect of the penetration decay scale of the Stokes drift (δ) and the misalignment between the wind stress and Stokes drift (θ_{ww}). The effect of the wind–wave angle of misalignment is guided by a set of idealized Large Eddy Simulations (LES) and the Langmuir Turbulence (LT) parameterization is developed based on LES of the ocean surface boundary layer at Ocean Weather Station Papa, for a period of 20 days under observed atmospheric and oceanic conditions. The KPP-LT model is implemented in the Navy Coastal Ocean Model (NCOM) and compared to in situ oceanographic measurements, LES and other Second Moment Closure (SMC) schemes available in NCOM, namely the model of Kantha and Clayson (2004) and Harcourt (2013, 2015). Comparisons with temperature observations suggest better performance of the KPP-LT model over SMC models within the boundary layer, which are supported by comparisons of inertially averaged eddy viscosity profiles estimated from LES.

1. Introduction

Ocean models based on the Reynolds Averaged Navier Stokes (RANS) equations use turbulence parameterizations to model the effect of unresolved motions on the mean flow. Turbulence models aimed at simulating the dynamics of the upper ocean determine the extent and relative influence that surface fluxes (heat and freshwater) and temperature distributions have on turbulent motions and how these redistribute momentum and heat. In the past few decades Langmuir turbulence (LT) has been recognized as an important source of turbulent energy in the upper ocean, significantly affecting the mean velocity and scalar flux profiles within the mixed layer (McWilliams et al., 1997, 2012). Although LT is now regarded as a contributing and often dominant factor driving turbulent processes that transport heat and momentum in the upper layers of oceans and lakes, global simulations using different LT closure schemes show significant discrepancies in the resulting temperature distributions (Li et al., 2019). Several different parameterizations have been proposed based on Second Moment Closure (SMC) models (e.g., Kantha and Clayson, 2004; Harcourt, 2013, 2015) and models based on the K-Profile Parameterization (KPP; McWilliams and Sullivan, 2000; Smyth et al., 2002; Van Roekel et al., 2018; Li and Fox-Kemper, 2017) to simulate the effects of LT. This study aims to assess the performance of different turbulent parameterization models that seek to simulate the effects of LT using the Navy Coastal Ocean Model (NCOM) under realistic forcing conditions, and propose a parameterization for the enhancement (i.e., the additional turbulent mixing) of the turbulent eddy viscosity in the presence of LT based on Large Eddy Simulations (LES) forced by observed wind and waves. The proposed model presented here (hereafter KPP-LT) is based on the KPP model (Large et al., 1994) as well as subsequent model improvements that account for LT (e.g., Smyth et al., 2002; Li and Fox-Kemper, 2017), and further attempts to take into account the effects of wind–wave angle of misalignment (Van Roekel et al., 2012) and Stokes drift decay scale (Kukulka and Harcourt, 2017). We find that the effect of misaligned Stokes drift and wind direction has significant impact on the diagnosed eddy viscosity profiles in idealized LES under weakly convective conditions. This is obscured in realistic LES configurations where strong convection is often dominant over LT, but important differences in turbulent intensities are still observed between aligned and misaligned wind–waves in realistic LES experiments (Fan et al., 2020). To assess the overall performance of the models, results are validated with observed sea surface temperature (SST) and mixed layer depth (MLD), which provide a bulk measure of the total mixing strength. However, we also emphasize the shape and magnitude of inertially averaged eddy viscosity profiles to elucidate local mixing effects,

* Correspondence to: Marine Science, The University of Southern Mississippi, Stennis Space Center, MS 39529, United States of America.
E-mail address: Miguel.solano@usm.edu (M. Solano).

https://doi.org/10.1016/j.ocemod.2022.101958
Received 22 July 2020; Received in revised form 11 January 2022; Accepted 15 January 2022
Available online 20 January 2022

especially in contrast to SMC models. Although we recognize that non-local transport effects are important, we focus on local transport since the models considered here formulate fluxes as downgradient (Large et al., 2019a,b).

A drawback of some turbulence closure models attempting to simulate the effects of LT in the ocean is the use of idealized LES experiments in the development of the model parameterization and tuning of model constants. These approximations are useful because they significantly reduce the complexity of ocean dynamics that facilitates the development of turbulence parameterizations and are necessary in understanding the dynamics of turbulent components individually. However, in practice ocean models using turbulence parameterizations developed under idealized conditions are expected to simulate ocean dynamics under realistic forcing conditions accurately with the implication that the ocean model solution is only weakly affected by these approximations. For example, the model developed by Kantha and Clayson (1994, 2004) tunes its constants to constant forcing simulations. In contrast, KPP models are more empirical in nature, using ocean observations to tune model constants. For example, the KPP of Large et al. (1994) uses Ocean Weather Station Papa (OWS-P) data in the original formulation. By tuning model constants to match observations the KPP scheme also has the downside of obscuring physically relevant effects, such as LT, which results in ocean models including unknown effects implicitly. Additionally, turbulence models may be biased towards the conditions under which they were developed, for example the LT parameterization by Reichl et al. (2016) that aims to simulate the dynamics of the ocean under hurricane conditions in which rapid ML deepening is expected yields good results under those conditions but significantly overestimates the mixed layer deepening in global simulations (Li et al., 2019). Therefore, turbulence models may benefit from being developed and tuned under the conditions that they are expected to simulate. Due to the large computational cost associated with high-resolution LES simulations, we choose to follow similar studies (Large et al., 2019a) to test and tune our parameterization under a wide range typical oceanic forcing conditions using surface fluxes computed from *in situ* observations.

More recently numerical LES experiments have addressed some of the complexities of ocean conditions, namely characterizing waves from an observed spectrum, non-constant wind forcing, and misaligned wind–waves. Failing to account for directional wave spreading and multidirectional wave effects can lead to overestimating the mean Stokes drift magnitude by 20%–40%, in addition to a directional veer with depth (Webb and Fox-Kemper, 2015). Characterizing broadband waves with a Langmuir number based on a Stokes drift profile is a significant complication from a modeling standpoint but appears to provide sufficient information about the wave forcing to be an effective independent variable (Large et al., 2019a). Numerical studies under tropical cyclone conditions show the importance of explicitly including sea-state dependent impact of LT, especially wind–wave misalignment (Reichl et al., 2016), and further suggest the use of Lagrangian instead of Eulerian currents to characterize the combined wind–wave effects (Van Roekel et al., 2012). Intercomparison of the most recent KPP modifications (Van Roekel et al., 2018; Li et al., 2019) clearly show that there is no clear way to characterize wave effects under all possible situations, and significant uncertainty remains regarding the nonlocal flux parameterization. Due to these uncertainties, in our study we choose to focus on the local flux parameterization and follow the suggestions from recent literature (Van Roekel et al., 2018; Li et al., 2019; Large et al., 2019a) to test and tune our parameterization under a wide range typical oceanic forcing conditions using surface fluxes computed from *in situ* observations.

This study presents the results of LES experiments at Ocean Weather Station Papa (hereafter OWS-P), during a 20-day period with a range of oceanic and atmospheric conditions representative of the combined Langmuir and convective turbulence dominant in the global ocean (Li et al., 2019; Fig. 12). The model is initialized by measured temperature and salinity, with surface fluxes computed from observed wind and wave measurements. Experiments with and without the effect of LT are performed to elucidate the enhancement of turbulence in the presence of the wave generated Stokes drift. These simulations are used to develop a model for the enhancement of the eddy viscosity brought by the presence of LT, that is, instead of parameterizing the eddy viscosity (K) we aim to parameterize the difference in eddy viscosity (ΔK) between simulations with and without wave forcing. The parameterization is based on the non-local KPP scheme (Large et al., 1994) now commonly used in ocean models, where we reconsider the original assumptions and approximations made by the authors and how they stand up to the numerical LES experiments under realistic forcing conditions. In addition to the enhancement of turbulent energy and modifications to the turbulent velocity scale (w_x) as suggested previously (McWilliams and Sullivan, 2000; Smyth et al., 2002), McWilliams and Sullivan (2000) first attempted to account for LT in KPP by introducing an enhancement factor to the turbulent velocity scale based on the turbulent Langmuir number La_t (McWilliams et al., 1997). Smyth et al. (2002) improved their scheme by adding a stratification effect to restrain/magnify the turbulence enhancement under weak/strong stratification conditions. To account for the effect of misaligned wind and waves, Van Roekel et al. (2012) proposed a projected Langmuir number reflecting the effect of wind–wave misalignment angle. While these studies improved the representation of boundary layer turbulence in our ocean circulation models, they all suggest enhanced turbulence with LT under all conditions. In this study, reduced turbulence was observed at large wind–wave misalignment, thus we attempt to better represent the effects of the wind–wave angle of misalignment that not only enhance mixing at smaller angles but can also reduce mixing at large angles.

NCOM was used by the Naval Oceanographic Office (NAVOCEANO) for operational global simulations and is still currently used at the Naval Research Laboratory (NRL) and by the Fleet Numerical Meteorology and Oceanography Center (FNMOC) for regional domains. Through this study, the original KPP scheme (Large et al., 1994) is implemented in NCOM for the first time, and the implementation will be validated without the effects of LT or any additional modifications (Large et al., 1994) against observations. The performance of the original KPP scheme will also be compared with the Mellor–Yamada level 2.5 (1982) and the Kantha and Clayson (1994) models. The new KPP-LT scheme presented here is then compared with other LT parameterizations, namely the SMC models by Kantha and Clayson (2004), Harcourt (2015) and the more recent KPP model of Li and Fox-Kemper (2017). Performance is evaluated by comparing the eddy viscosity from NCOM with LES estimates, and further validated with observed SST and MLD.

This paper is organized as follows. Section 2 outlines the methodology, idealizations typically made in LES experiments, and their limitations in describing the real ocean. This section also provides a description of our LES model and experiments, which includes two simulations at OWS-P under realistic forcing conditions and a set of idealized simulations forced with different wind–wave misalignment angles. Section 3 describes the KPP-LT parameterization, including the relevant physical parameters used and their non-dimensional scaling. Section 4 presents the results from our NCOM simulations at OWS-P which include our KPP-LT model, the KPP parameterization of Li and Fox-Kemper (2017), the SMC models of Kantha and Clayson (2004) and Harcourt (2015), compared with our LES experiments and observations. Section 5 presents a summary of this study, our interpretations on the model results, limitations and future work.

2. Method

A critical component in the study and development of turbulent parameterizations for the Oceanic Surface Boundary Layer (OSBL) is the use of LES that explicitly calculates the grid-scale Reynold stresses and model Sub-Grid Stresses (SGS; Moeng, 1984). LES that solve the

phase averaged, Craik–Leibovich, equations have been shown to quantitatively simulate important characteristics of LT observed in the ocean, namely decreased downwind mean shear ($\partial_z u$) (e.g., Price and Sundermeyer, 1999), an increase of near-surface crosswind/wave normalized turbulent kinetic energy (TKE; $(v_{rms}/u_*)^2$; e.g., Gargett et al., 2004) and mixed layer vertical TKE ($(w_{rms}/u_*)^2$; e.g., D'Asaro, 2001), thus providing a good benchmark for parameterizations used in large scale circulation models (Zikanov et al., 2003). Idealized LES studies have been used to characterize LT under a wide range of oceanic conditions, including steady moderate winds with weakly convective surface forcing (Skyllingstad and Denbo, 1995; McWilliams et al., 1997; Li et al., 2005), tropical cyclones (Sullivan et al., 2012; Reichl et al., 2016) and very strong swells (McWilliams et al., 2014). In this study we emphasize the importance of using observed oceanic and meteorological condition in LES simulations for the purpose of parameter development for turbulence closure models.

2.1. Large eddy simulations

The LES model used here solves the filtered Craik–Leibovich (Craik and Leibovich, 1976) momentum and continuity equations:

$$\frac{D\vec{u}}{Dt} + f\hat{z}\times\left(\vec{u}+\vec{u_s}\right) = -\nabla\pi - g\hat{z}\left(\frac{\rho}{\rho_0}\right) + \vec{u_s}\times\vec{\omega} + SGS \tag{1}$$

$$\frac{D\rho}{Dt} + \vec{u_s}\cdot\nabla\rho = SGS \tag{2}$$

$$\nabla\cdot\vec{u} = 0 \tag{3}$$

where g is the gravitational acceleration, $D/Dt = \partial_t + \vec{u}\cdot\nabla$. The Eulerian velocity vector is denoted by $\vec{u} = (u, v, w)$, the resolved vorticity is $\vec{\omega} = (\omega_x, \omega_y, \omega_z) = \nabla\times\vec{u}$, the Stokes drift velocity is $\vec{u_s} = (u_s, v_s, 0)$, ρ is the water density with ρ_0 being its reference density, f is the Coriolis parameter, $\pi = p/\rho_0 + \frac{1}{2}\left[|\vec{u}+\vec{u}_s|^2 - |\vec{u}|^2\right]$ is a generalized pressure and $\hat{z}$ denotes the vertical coordinate. The prognostic equation for the subgrid scale (SGS) model in the LES takes the same form as the turbulent kinetic equation except the fluxes are parameterized instead of being resolved. The details on the SGS model can be found in Sullivan et al. (2007) and the Appendix.

2.2. Model idealizations

In the context of turbulent parameterizations for the OSBL three approximations are commonly used in LES experiments seeking to understand the effects of LT: steady-state surface forcing, monochromatic waves and aligned wind–wave directions. Experiments using steady-state surface forcing of heat and momentum fluxes seek equilibrium solutions to understand the individual contributions from shear, convection and LT to the total TKE budget and their effects on the equilibrium velocity and temperature distributions. Although quasi steady states have been observed in the ocean their persistence over long term periods is questionable. Consequently, LES experiments assuming a steady-state surface forcing are mostly useful from a theoretical standpoint but have limited applicability to the real ocean. In the study of Kantha and Clayson (Kantha and Clayson, 2004), the authors replicate the idealized conditions in the LES experiments by McWilliams et al. (1997) in order to tune the model parameter (E_6), which sets the relative contribution of the Craik–Leibovich Vortex Force term in the prognostic equation for $q^2 l$ and consequently the turbulent eddy viscosity ($K_m = S_m q l$), where S_m is a stability function for momentum, q is the turbulent velocity scale and l is the turbulent length scale (Mellor and Yamada, 1982; Harcourt, 2015). When setting $E_6 = 1$, both TKE and dissipation levels agree well with LES results by McWilliams, but the turbulent eddy viscosity is underestimated. Kantha and Clayson (2004) choose to set $E_6 = 7.2$ (see Kantha et al., 2010) in order to match the turbulent eddy viscosity to LES estimated values, presumably overestimating TKE and dissipation levels. While tuning the model constants for the Mellor–Yamada level 2.5 model (Mellor and Yamada, 1982), the basis of all general length scale models (Umlauf and Burchard, 2003) such as the model by Kantha and Clayson (2004), the authors warn that a bias to any one set of data will result in that set being well predicted while being less skillful for other sets. Invoking steady surface forcing is therefore useful in the development of turbulent parameterizations to provide a theoretical framework from the equilibrium solutions and low-order statistics, but ultimately ocean models should be tuned under realistic surface conditions to avoid possible biases towards the (unrealistic) stationary state. Although the stationary (i.e. time-independent) solution is certainly important and physically relevant, ocean models are significantly affected by the transient conditions ubiquitous in the real ocean.

Another idealization commonly made in LES experiments to study LT is the monochromatic wave approximation that facilitates the estimation of the Stokes drift. Even in this idealized form, a surface gravity wave field as a steady, monochromatic, deep-water wave (equation. 2.4 in McWilliams et al. (1997)), the Stokes drift (u_s) is a function of two variables: the surface Stokes drift (U_s) and its wavelength ($L = 2\pi/k$; k is the wave number) with the implication that the Stokes drift profile can only be uniquely defined by using a minimum of two parameters. Consequently, the turbulent Langmuir number ($La_t = \sqrt{u_*/U_s}$), where u_* is the water side friction velocity, is apt to characterize the effects of LT under this idealization (i.e., monochromatic waves), but shows no explicit sensitivity to the Stokes drift decay scale or the angle between Stokes drift and wind stress. In contrast, the Hoenikker number defined as $Ho = 4B_0/U_s\delta u_*^2$ (Li et al., 2005), where B_0 is the surface buoyancy flux and $\delta = (2k)^{-1}$ is the Stokes drift decay scale (or e-folding scale, also referred to as penetration depth), does take into account the wavelength through δ to measure the relative effects of convective and Langmuir turbulence. The monochromatic wave approximation has been made mostly on grounds of simplicity and the assumption that turbulence dynamics in the OSBL are only weakly dependent on the dimensionless depth ratio kh (Li et al., 2005), where k is the wavenumber of a monochromatic wave with Stokes drift decay length δ, and h is the boundary layer depth (BLD). However, more recent studies (McWilliams et al., 2014; Kukulka and Harcourt, 2017) show important differences in turbulent statistics and buoyancy entrainment rates between short equilibrium wind–waves and longer swell waves. LES experiments of LT in pure wind seas (Harcourt and D'Asaro, 2008) show that using a scale-equivalent monochromatic wave does not accurately reproduce the results using a full-surface wave spectrum with the same penetration depth. In their study, Harcourt and D'Asaro suggest a surface layer-averaged Langmuir number (La_{SL}) to consider the different penetration depths of the Stokes drift, estimated from both monochromatic and broadband spectra. Further numerical experiments show that under nonequilibrium swell conditions the OSBL does not restratify despite low wind and strong solar radiation (Kukulka et al., 2013) and wind–wave equilibrium can significantly affect the vertical distribution of passive buoyant tracers through near-surface enhanced TKE due to wave breaking and LT (Kukulka and Brunner, 2015). Therefore, turbulence models developed and tuned under the assumption of a monochromatic wave field cannot be expected to perform well in the real ocean, and the non-dimensional numbers used to characterize LT under these idealized conditions have significant limitations in characterizing LT under realistic forcing conditions.

Perhaps the most commonly used approximation in LT parameterizations is the assumption that the wind stress and Stokes drift act in the same direction. In this approximation the waves are assumed to be in equilibrium with the local wind (i.e., $C_p/U_{10} = 1.2$), where C_p is the phase speed of the waves at the peak of the wave spectrum and U_{10} is the wind velocity at 10 m height. The wave number is usually used to estimate the Stokes drift when there is no observed or modeled data of the wave field. However, surface gravity waves often propagate long distances in form of swells where the wind is rarely in equilibrium with the waves (Hanely et al., 2010). LES experiments in swell show an amplification of the Lagrangian-mean current, an

enhancement of the turbulent variance and buoyancy entrainment rate from the pycnocline compared to an equilibrium wind–sea (McWilliams et al., 2014). The relative importance of wind and wave directions is obscured by the difficultness in measuring turbulent shear and Stokes drift simultaneously, but the study of Kantha et al. (2010) suggests a scaling proportional to the dot product of Stokes drift and wind stress at the surface. LES experiments simulating the effect of misaligned Stokes drift and wind direction show that the axial direction and rotation of the Langmuir cell pairs changes significantly with the wind–wave angle, as well the vertical variance and scaling of the turbulent Langmuir number (Van Roekel et al., 2012). These findings are supported by LES experiments of tropical cyclones, which show that misaligned winds and waves result in vertical momentum fluxes that counter the gradient of the Stokes drift so that the potency of LT depends on the turbulent Langmuir number, the wind-Stokes drift alignment and the relative penetration scale (kh) of the Stokes drift (Sullivan et al., 2012). Attempts to include the effect of wind–wave misalignment in LT parameterizations suggest the use of the Lagrangian velocity ($u_L = u_s + u$) and shear to direct part of the momentum flux down the Stokes shear (McWilliams et al., 2012; Reichl et al., 2016).

2.3. LES at OWS-P

The first set of LES experiments consists of two simulations at OWS-P, one with the effect of LT, and the other without the effect of LT. Unless otherwise specified, simulations with the effect of LT will be labeled "LT". For example, the difference in eddy viscosity between simulations with LT and without LT are computed as $\Delta K = K_{LT} - K$, where the eddy viscosity from simulations without LT are subtracted from simulations with the effect of LT.

OWS-P is located 850 miles off the British Columbia, Canadian coast at $145°E$ and $50°N$. Simulations span a period of 20 days, starting on November 14, 2011 at 1 UTC and ending on December 4, 2011 at 1 UTC. The horizontal domain is set to be 300 m in both directions, which is 4–5 times of the mixed layer depth that varied between 60 m to 80 m during our simulation period and thus is wide enough to permit multiple coherent largest scale structures to develop independent of the periodic side wall boundary conditions imposed. The vertical extent of the domain is 200 m, which is more than twice of maximum mixed layer depth and thus can permit a smooth transition between the turbulent and stably stratified layers below. A vertical grid with 128 grid points stretched towards the surface starting at 0.2-meter depth is used to better resolve the surface fluxes and the rapid vertical decay of the Stokes drift profiles.

The model starts from rest ($\vec{u} = 0$) with temperature and salinity profiles initialized from measurements at 17 levels from 1 meter to 300 meters depth, which are linearly interpolated to the vertical grid. Both temperature and salinity profiles at initialization are vertically uniform in the upper 60 meters with a sharp thermocline/halocline at the base of the mixed layer. Hourly wind stress ($\vec{\tau}$) was calculated from observed 10-m winds using the vectorized COARE 3.5 algorithm modified from Fairall et al. (2003), and net heat flux (Q) was computed using the sensible and latent heat fluxes from the COARE 3.0 bulk algorithm as well as observations of the net shortwave and longwave radiation.

Concurrent detailed two-dimensional wave spectra, $E(\sigma,\theta)$, were collected near ocean station papa by the Applied Physics Laboratory at the University of Washington using a 0.9 m Datawell directional waverider (Thomson et al., 2013). Where σ and θ are the frequency and direction of the spectra. The hourly Stokes drift profile time series were computed following Kenyon (1969):

$$\vec{u}_s(z) = 2\iint \omega\vec{k}E(\omega,\theta)e^{-2kz}d\sigma d\theta \tag{4}$$

where $\vec{k}$ is the wave number vector of the spectra.

Surface fluxes and Stokes drift are shown in Fig. 1 along with the wind–wave angle of misalignment (θ_{ww}) and Stokes e-folding depth (δ). Note that during this 20-day period wind stress ranges between 0 and 1.2 Pa (0–25 ms^{-1}) and heat flux ranges from -450 Wm^{-2} (strongly convective) to 175 Wm^{-2} (stable) providing a wide range of surface forcing conditions for testing our model. The dashed lines in Fig. 1 indicate the 10 inertial periods ($T1$–$T10$) from November 16 at 07:12 UTC to November 22 at 19:25 UTC used to guide our parameterization, which is then tested for the entire 20-day period.

2.4. LES with varying wind–wave angles

The second set of LES experiments consists on a suite of idealized experiments with wind–wave misalignment angles ranging from 0 to 135 degrees, used to guide the LT parameterization under different angles of misalignment. Stratified ocean initial conditions are prescribed for the idealized experiments with a constant density layer in top 20 m. Below that layer, stable stratification of $d\theta/dz = 0.01$ K/m is prescribed with a constant thermal expansion coefficient $\alpha = 2\times10^{-4}$ K^{-1}. Constant forcing is applied for all experiments following McWilliams et al. (1997) with wind stress $\tau = 0.037$ Nm^{-2} (corresponding to a wind speed of about 5 m s^{-1}), a weak heat flux into the ocean of $Q = -5$ Wm^{-2}, and a Stokes drift profile from a sinusoidal wave with an amplitude of 0.8 m and length of 60 m corresponding to Stokes drift with surface value of $U_s = 0.068$ m s^{-1}. This implies a La_t equal to 0.3. The $\hat{x}$ direction in the model is defined as the along-wind direction. The boundary layer environment is uniformly rotating for all experiments, with $f = 8.5867\times10^{-5}$ s^{-1}, corresponding to $36.17°$ N latitude. All model runs are spun up from rest to a statistical equilibrium state after one inertial period (~20.3 h). For more details on this set of simulations the reader is referred to Fan et al. (2020).

2.5. TKE budget

We start by considering the TKE budget to gain insight on the relative importance of each term responsible for vertical mixing. The horizontal domain averaged TKE equation can be written as:

$$\frac{\partial e}{\partial t} = T_t + P_{shear} + P_{buoy} + T_{pressure} + P_{Stokes} - \varepsilon + SGS \tag{5}$$

where,

$T_t = -\frac{1}{2}\left(\frac{\partial\langle u'^2w'\rangle}{\partial z} + \frac{\partial\langle v'^2w'\rangle}{\partial z} + \frac{\partial\langle w'^2w'\rangle}{\partial z}\right)$ is the turbulent transport term,

$P_{shear} = -\langle u'w'\rangle\cdot\frac{\partial\langle u\rangle}{\partial z} - \langle v'w'\rangle\cdot\frac{\partial\langle v\rangle}{\partial z}$ is the shear production term,

$P_{buoy} = \alpha g\langle\theta'w'\rangle - \beta g\langle s'w'\rangle$ is the buoyancy production term,

$T_{pressure} = -\frac{1}{\rho_0}\frac{\partial\langle p'w\rangle}{\partial z}$ is the pressure transport term,

$P_{Stokes} = -\langle u'w'\rangle\frac{\partial u^{Sx}}{\partial z} - \langle v'w'\rangle\frac{\partial u^{Sy}}{\partial z}$ is the Stokes production term,

e is the total TKE, ε is the kinetic energy dissipation rate, and SGS is the subgrid-scale contribution. The angle bracket in the above equations represents horizontal domain average, the superscript prime denotes a departure from the mean value.

The TKE budget for the LES experiments with and without the effect of LT at OWS-P are shown in Fig. 2, averaged over the ten inertial periods shown in Fig. 1. In the absence of LT, the balance is between shear production, buoyancy and dissipation, but in the presence of LT Stokes production becomes the dominant source of energy at the surface, followed by shear production, while transport terms that are negligible in simulations without LT now play a minor role. The contribution from shear production when LT is present decreases because vertical gradients of velocity decrease faster than the increase in turbulent fluxes, commonly referred to as the "anti-Stokes" effect (Haney, 2015; Pearson et al., 2018). The turbulent transport and pressure terms are

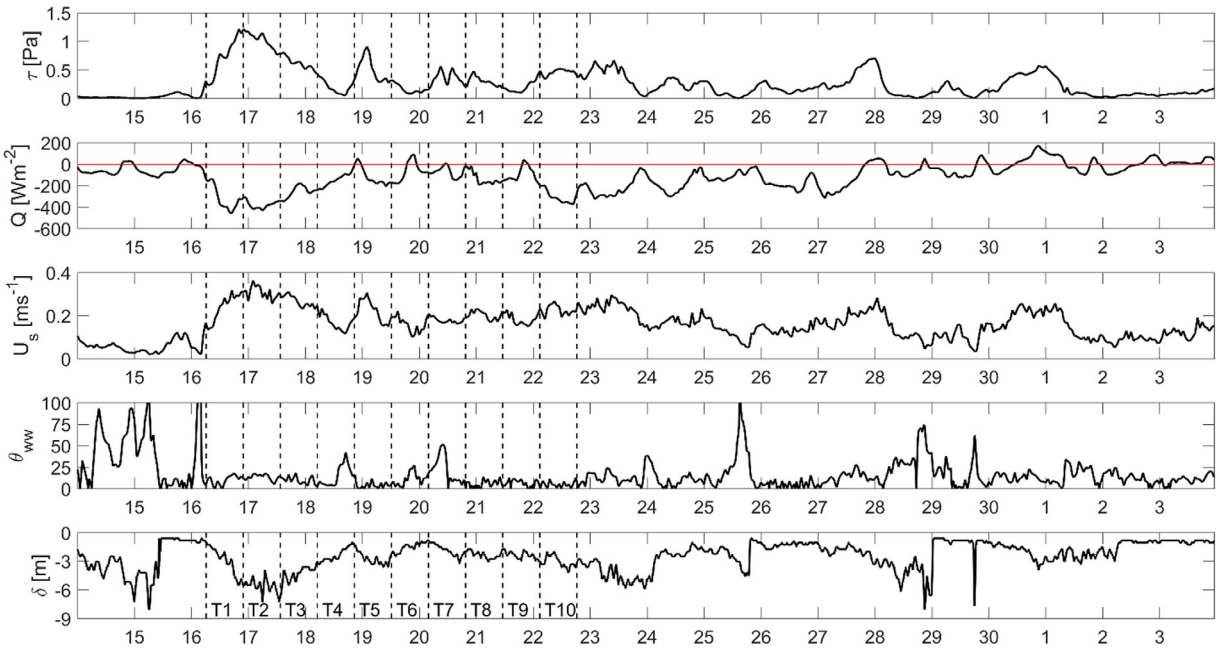

Fig. 1. Surface forcing at OWS-P. From top to bottom: wind stress (τ), net heat flux (Q), surface Stokes drift (U_s), wind–wave angle (θ_{ww}), Stokes drift e-folding depth (δ). The dashed lines show the period used to compute inertial averages (labeled T1 to T10).

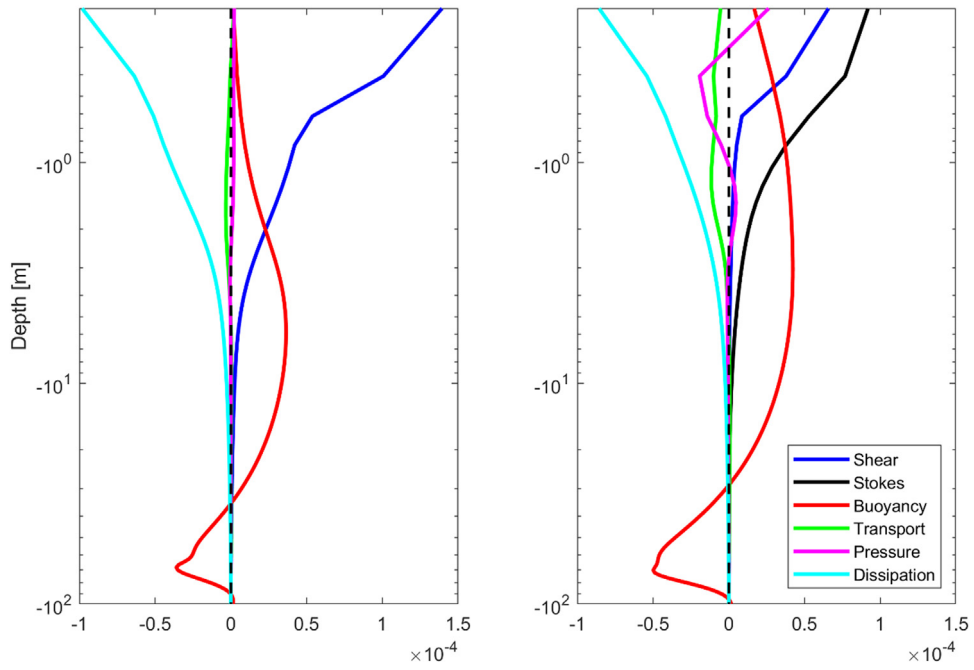

Fig. 2. Vertical Turbulent Kinetic Energy budget at Ocean Weather Station Papa from the LES model averaged over 10 inertial periods (6.5 day period). (Left) Without LT. (Right) With LT. Each term of the budget specified in the label is defined in Eq. (4).

also significantly larger in the simulation with LT while the dissipation is slightly reduced, suggesting that the excess of available energy at the near surface is transported downwards instead of being dissipated at the surface. At the surface, Stokes production is the largest source of TKE but buoyancy term is dominant in the bulk of the mixed layer, which is easier to observe in a linear plot (not shown). Buoyancy production also increases slightly, suggesting Stokes shear and buoyancy work together to increase vertical mixing. Using these model results and dimensional analysis, we now consider various physical parameters that may contribute to the enhanced vertical mixing by LT.

3. Langmuir turbulence parameterization

In this study, we aim to parameterize the *enhancement* in vertical mixing brought by the inclusion of LT in turbulent models which already account for shear and convection. Hence, our variable of interest is $\Delta K = K_{LT} - K$ where K_{LT} is the eddy viscosity in the presence of LT and K is the eddy viscosity due to shear and convection only. Posing the problem in this manner allows this parameterization to be added to any already existing turbulent closure model that neglects the effect of LT. Additionally, under certain conditions the difference in eddy viscosity

is allowed to be negative for cases in which the presence of the Stokes drift reduces the turbulent intensity.

We model the eddy viscosity without the effect of LT exactly as in Large et al. (1994):

$$K(\sigma) = h w_m(\sigma) G(\sigma) \tag{6}$$

Where h is the BLD, w_m is a turbulent velocity scale, G is a nondimensional shape function and $\sigma = z/h$ is a nondimensional vertical coordinate that varies from 0 at the surface to 1 at the base of the boundary layer, where z is the distance from the surface. Eq. (6) is a common way to calculate eddy viscosities and diffusivities in one equation. In some models the non-local flux is computed differently, for example in Large et al. (1994) it is zero for momentum but non-zero for scalars (temperature/salinity). In our study we focus only on the local (down-gradient) component (K, first term Eq. (7)) and treat eddy viscosity/diffusivity in the same way, so it is not necessary to discuss eddy viscosities and diffusivities separately. This also keeps the Prandtl number unaltered and equal to w_m/w_s in accordance to Troen and Mahrt (1986). This is discussed in Appendix B from Large et al. (1994).

For details of this parameterization the reader is referred to Large et al. (1994). Note that we implemented the KPP scheme in NCOM as it was originally presented and did not tune it for our application. Since the model was also originally tuned to OWS-P observations it provides a good benchmark for comparison, but this also implies that the effect of LT is implicitly accounted for to some degree.

For simplicity, we apply the parameterization to both the eddy viscosity and diffusivity in the same fashion.

3.1. Definitions

First, we provide a formal definition for three important physical parameters used in the parameterization and model validation: eddy viscosity, MLD and BLD. The eddy viscosity (diffusivity) is used in ocean models to parameterize the vertical turbulent momentum (heat) fluxes as:

$$\overline{w'\lambda'} = -K_\lambda \partial_z \overline{\lambda} + \Gamma_\lambda \tag{7}$$

Where $(\overline{w'\lambda'})$ refers to the turbulent flux of a quantity λ, which may be specified for momentum $(\overline{u'w'}, \overline{v'w'})$ or scalars such as temperature $(\overline{w'\theta'})$, $\partial_z \overline{\lambda}$ is the mean vertical gradient and Γ_λ represents any flux not proportional to the local gradient (Li et al., 2019). For the purposes of this study the eddy viscosity (K) refers specifically to the turbulent momentum flux, and we diagnose it in LES as the scalar eddy viscosity:

$$K = \frac{\sqrt{\overline{u'w'}^2 + \overline{v'w'}^2}}{\sqrt{\left(\frac{\partial u}{\partial z}\right)^2 + \left(\frac{\partial v}{\partial z}\right)^2}} \tag{8}$$

Additionally, we omit the non-local flux Γ_λ in Eq. (7) following Large et al. (1994).

The oceanic BLD is defined from a physical standpoint as the limit to which the largest boundary layer eddies can penetrate in the vertical direction, which depends on the surface forcing, oceanic buoyancy $(B(z))$ and the mean velocity $(V(z) = \|\vec{u}\|)$ profiles. In KPP models the BLD is defined as the smallest distance (z) at which the bulk Richardson number (Ri_b) equals a critical value Ri_c,

$$Ri_b = \frac{\left(B_r - B(d)\right) z}{\left(V_r - V(z)\right)^2 + V_t^2(z)} \tag{9}$$

where B_r and V_r are the near surface reference buoyancy and velocity respectively, computed by averaging each respective profile over the surface layer $(h_{SL} = \epsilon h)$ and the term V_t^2 is a velocity scale which accounts for the unresolved velocity shear. Note that fluxes should be about 20% of their surface value at the surface layer depth and approach linearly as z becomes small, which has been taken to be about 10% of the boundary layer depth, a value originally taken from atmospheric boundary layer values (Tennekes, 1973; Large et al., 1994). We find that this is roughly a good estimate in our simulations and therefore, we choose to set $\epsilon = 0.1$ when computing the near surface reference buoyancy and velocity in (8). However, when computing the surface-layer averaged Langmuir number (defined later) the averaging is taken to be 20% of the mixed layer, in both cases we choose these definitions to be consistent with the original work (Large et al., 1994). For all of our analyses we use a critical Richardson number $Ri_c = 0.3$. In simulations without the effect of the Stokes drift, the velocity scale V_t^2 is parameterized using Eq. (23) from Large et al. (1994):

$$V_t = \frac{C_v \left(-\beta_T\right)^{\frac{1}{2}}}{Ri_c \kappa^2} \left(c_s \epsilon\right)^{-\frac{1}{2}} d N w_s \tag{10}$$

Where $C_v = 1.6$ is the ratio of stratification frequency N at the interior and the entrainment depth, β_T is the ratio of entrainment flux to surface buoyancy flux, w_s is the turbulent velocity scale for scalars, and $\kappa = 0.4$ is Von Karman's constant. In simulations that include the Stokes drift it is parameterized using Eq. (26) from Li and Fox-Kemper (2017).

$$V_t = \frac{C_v N w_s d}{Ri_c} \left[\frac{0.15 w_*^3 + 0.17 u_*^3 \left(1 + 0.49 La_{SL}^{-2}\right)}{w_s^3}\right]^{1/2} \tag{11}$$

The surface layer averaged Langmuir number (La_{SL}; Harcourt and D'Asaro, 2008) is defined as:

$$La_{SL} = \sqrt{\frac{u_*}{\left(\left\langle u^S \right\rangle_{SL} - u^S_{ref}\right)}} \tag{12}$$

Where the (u^S_{ref}) is a reference velocity equal to the Stokes drift velocity at $-0.765 h_m$, and the surface layer averaged velocity is defined as:

$$\left\langle u^S \right\rangle_{SL} = \frac{5}{h_m} \int_{-\frac{h_m}{5}}^{0} u^S dz \tag{13}$$

As we will discuss later, parameterization of the unresolved Stokes drift through the velocity scale V_t^2 as suggested by Li and Fox-Kemper (2017) is essential to estimate the BLD.

Finally, we define the MLD (h_m) as the depth at which the temperature changes by 0.2^0C from its surface value. In our simulations, this corresponds roughly to a change of 0.03 kg/m^3 from the surface, which shows better agreement in global simulations compared to other criteria de Boyer Montegut et al. (2004). For additional discussion on the difference between the MLD, BLD and other length scales relevant to scaling turbulence in the OSBL the reader is referred to Sutherland et al. (2014) and Pearson et al. (2018). As will be discussed later, all KPP parameterizations results show significant sensitivity to the computation of the BLD.

3.2. Scaling of LT: physical variables

A critical aspect of any model parameterization is to provide the proper scaling for the phenomena under study, which requires the identification of the relevant physical variables affecting the flow. The eddy viscosity K has units of m^2/s, is composed of two fundamental units: length and time. Using dimensional analysis, we can express the enhancement of the eddy viscosity as:

$$\Delta K = f(f_1, f_2, \ldots, f_n) \tag{14}$$

Where $\{f_1, f_2, \ldots, f_n\}$ are the most relevant physical variables affecting the enhancement in vertical mixing in the presence of LT. According to Monin–Obukhov similarity theory, the important turbulence parameters affecting the surface layer are the distance from the boundary (z) and surface fluxes $(\overline{w'\lambda'})$. The contribution from wind-forced turbulence (P_{shear}) is commonly scaled using the water-side friction velocity $(u_* = \sqrt{\tau/\rho_0})$ and buoyancy production (P_{buoy}) is usually scaled

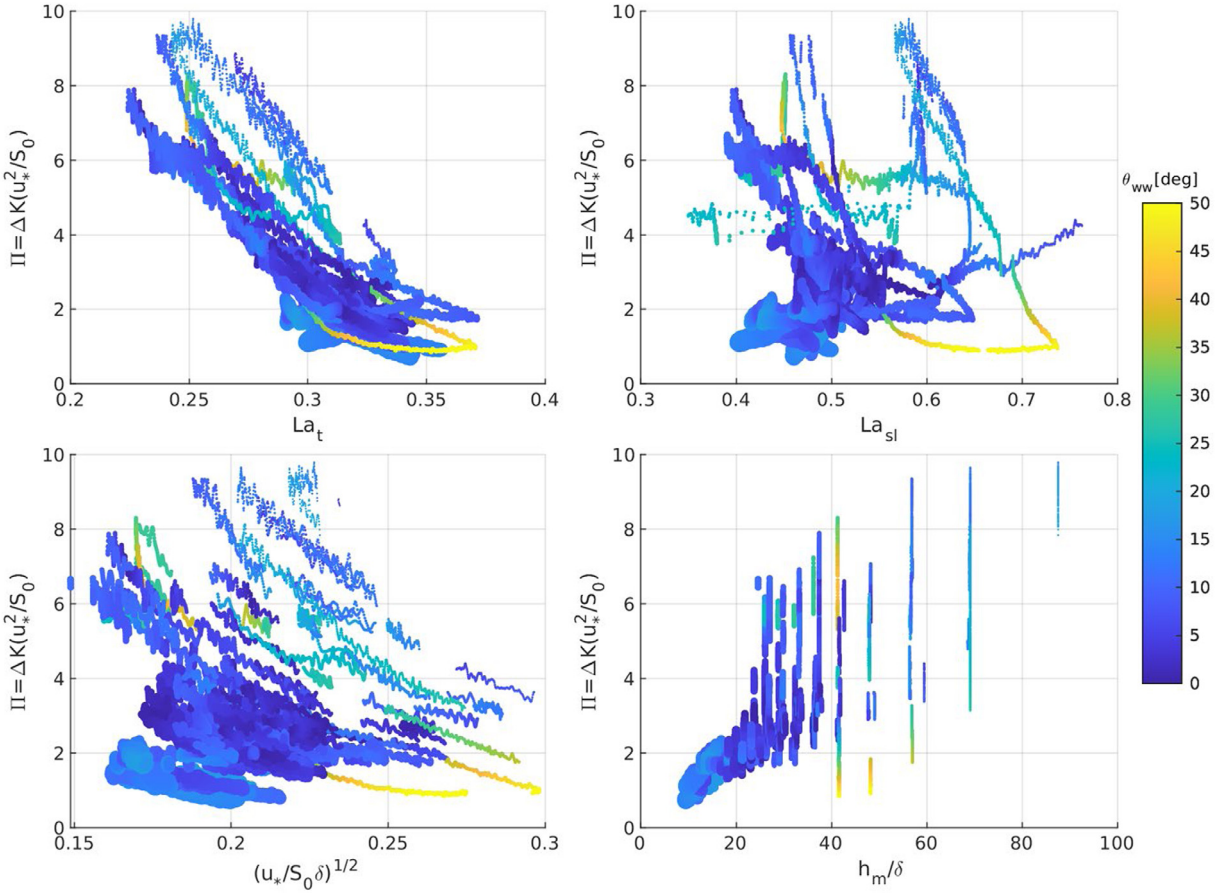

Fig. 3. Scaling of our dimensionless eddy viscosity (Π) with (top-left) the turbulent Langmuir number, (top-right) the surface layer averaged Langmuir number, (bottom-left) dimensionless parameter ($u_*/\delta S_0$), and (bottom-right) depth ratio (h_m/δ).

using the surface buoyancy flux (B_0) or Deardorff's convective velocity ($w_* = \left(-B_0 h\right)^{1/3}$). The relevant physical parameters used to describe the contribution from the Stokes drift (P_{Stokes}) is more complicated, but some LES studies suggest that the wave-forced turbulence should be scaled with a Langmuir velocity scale ($w_{*L} = \left(u_*^2 u_s\right)^{1/3}$) and a mixed layer depth h_m (Harcourt and D'Asaro, 2008; Grant and Belcher, 2009). This is in fact the most convenient way to scale the contribution from the Stokes drift, but it suffers from the same limitation as the turbulent Langmuir number in that it shows no explicit sensitivity to the Stokes drift depth scale such that wind (swell) waves with the same surface Stokes drift associated with shorter (longer) penetration depths will scale identically. To capture the effect of the Stokes penetration depth, we choose to scale the contribution from the Stokes drift using the depth scale (δ) and the Stokes shear at the surface (S_0). The stratification is considered through the MLD, so we can express the dimensional eddy viscosity difference as:

$$\Delta K = f(u_*, B_0, S_0, \delta, h_m) \tag{15}$$

3.3. Scaling of LT: dimensionless numbers

In order to find the appropriate dimensionless variables to be used in the parameterization, we start by non-dimensionalizing our variable of interest (ΔK). Since we chose the surface Stokes shear as the most relevant scale affecting Stokes production, we normalize our eddy viscosity difference as:

$$\Pi = \Delta K \left(\frac{S_0}{u_*^2}\right) \tag{16}$$

We now seek to scale the surface value of dimensionless eddy viscosity (Π) using the relevant physical parameters in Eq. (15). In Fig. 3, we show the scaling of our dimensionless eddy viscosity (16) during the ten inertial periods shown in Fig. 1, with the turbulent Langmuir number (McWilliams et al., 1997), the surface layer Langmuir number (Harcourt and D'Asaro, 2008), the depth ratio (h_m/δ) and the dimensionless parameter ($u_*/\delta S_0$). The turbulent Langmuir number, which provides a dimensionless ratio between shear and Stokes production at the surface, is in the range of 0.22–0.37 during the 6.5-day period plotted in Fig. 3 and the surface layer Langmuir number, which integrates the Stokes drift over the surface layer, is in the range of 0.35–0.75, neither of which yields a good scaling with Π. For short wind–waves of penetration depths of δ = 1–2 m, as indicated by the smaller size of the scatter markers in Fig. 3, show a different scaling than for deeper δ = 5–8 m waves. A similar scaling is observed with $u_*/\delta S_0$, due to the fact that $U_S \sim 1/\delta S_0$ so that this ratio is analogous to the turbulent Langmuir number. The depth ratio (h_m/δ) increases with Π, suggesting that the penetration depth is in fact a relevant physical parameter, but it also fails to scale with Π as the depth ratio increases over a certain threshold. To get a better scaling for Π with we obtain a new parameter by combining h_m/δ and $u_*/\delta S_0$ to form:

$$\left(\frac{u_*}{\delta S_0}\right)\left(\frac{\delta}{h_m}\right) = \left(\frac{u_*}{S_0 h_m}\right) = La_m \tag{17}$$

The scaling of this new modified Langmuir number (La_m) with the surface value of the dimensionless eddy viscosity (16) is shown in Fig. 4, which shows great improvement over those in Fig. 3. However, the scaling fails as the wind–wave angle of misalignment increases, suggesting that it is in fact a relevant parameter affecting vertical mixing in the ocean and must therefore be taken into account in our parameterization.

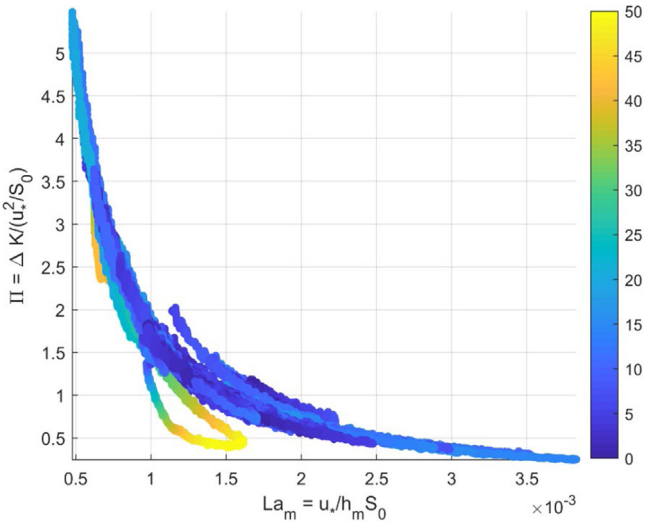

Fig. 4. Scaling of modified Langmuir number with non-dimensional eddy viscosity colored by wind–wave misalignment angle.

3.4. Effect of wind–wave misalignment

In this section, we use our idealized LES experiments described in Section 2.4 to guide the parameterization of the wind–wave angle of misalignment. As a starting point since our idealized LES experiments are performed under very similar conditions (i.e., weakly convective, monochromatic waves and a steady wind stress), we use the suggested enhancement by McWilliams and Sullivan (2000) to parameterize the effect of LT for the case of aligned wind–waves ($\theta_{ww} = 0$):

$$K_{LT}(\sigma) = hw_m(\sigma)\, G(\sigma) \left[1 + \frac{C_w}{La_t^4}\right]^{1/2} \tag{18}$$

Where C_w accounts for the effect of convection and is computed using Eq. (13) from Smyth et al. (2002). To account for the effect of wind–wave misalignment on the enhancement of eddy viscosity, we introduce a function $g(\theta_{ww})$ to parameterize the difference in eddy viscosity as:

$$\Delta K = (K_{LT} - K) g(\theta_{ww}) \tag{19}$$

Then, we compute the eddy viscosity difference $(K_{LT} - K)$ from our LES experiments as a function of the wind–wave angle, shown in Fig. 5 by the solid lines. In agreement with previous studies (e.g., Van Roekel et al., 2018), vertical mixing enhancement is maximum for aligned wind–waves ($\theta_{ww} = 0$) and decreases with increasing angle of misalignment. Results from our idealized LES experiments also suggest that at high wind–wave angles ($\theta_{ww} > 45°$) turbulence levels resemble simulations without LT (i.e., $\Delta K \approx 0$), and further increasing the misalignment ($\theta_{ww} > 60°$) results in lower turbulence levels ($\Delta K < 0$; Fan et al., 2020). This observation supports the idea that the wind–wave misalignment angle is an important factor affecting the scaling of dimensionless eddy viscosity with our dimensionless parameter La_m (Eq. (17)), which fails to scale after the wind–wave misalignment angle is greater than around 45 degrees (Fig. 4).

The parameterization of the difference in eddy viscosity using Large et al. (1994) for K and by McWilliams and Sullivan (2000) for K_{LT} (i.e., $K_{LT} - K$; dashed blue line) in Fig. 5 shows good agreement with our LES simulation for the case of aligned wind–waves (solid blue line).

Now we can derive the form of $g(\theta_{ww})$, hereafter called the wind–wave modulation function, by analyzing the eddy viscosity difference computed from LES and assuming that the reduction in vertical mixing is symmetrical along the direction of the wind, meaning that there is no difference in vertical mixing if the Stokes drift is misaligned to the right/left of the wind direction. Therefore, the wind–wave angle of misalignment has a range θ_{ww} = 0–180° and $g(\theta_{ww})$ should be symmetric about $\theta_{ww} = 0$. Additionally, since the eddy viscosity difference decreases faster at lower wind–wind wave angles (i.e., the difference from θ_{ww} = 0–30 is greater than θ_{ww} = 90–120), we assume $g(\theta_{ww})$ decays rapidly. With these constraints we choose a generalized form for the wind–wave modulation function:

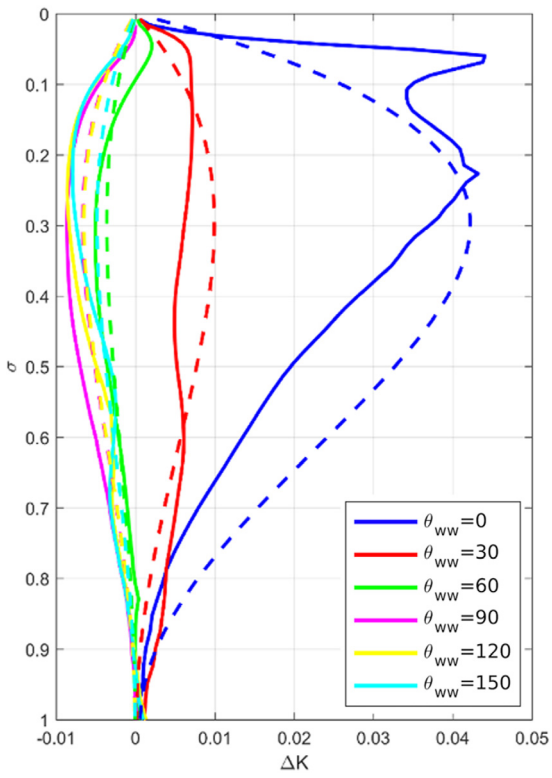

Fig. 5. Profiles of eddy viscosity difference between simulations with and without LT at different wind–wave misalignment angles. Solid lines are estimated from LES and dashed lines are calculated using the parameterization (Eqs. (16) and (18)).

$$g\left(\theta_{ww}\right) = c_1 e^{-|\theta_{ww}|} \cos(c_2 \theta_{ww} + c_3) \tag{20}$$

Where (c_1, c_2, c_3) are constants used to match the parameterization with the LES eddy viscosity difference, which we set using the following constraints:

- Enhancement of the difference is maximum at 0 degrees, so $g\,(0) = 1$
- Enhancement of the difference is 0 around 45 degrees, so $g\,(\sim 45) = 0$
- Maximum reduction is around 90 degrees, so $g\,(\sim 90) = \min\,(g) < 0$

The wind–wave modulation function is allowed to be negative at high wind–wave angles to account for the negative viscosity difference observed in LES (Fig. 5). The wind–wave modulation function, shown in Fig. 6, takes the final form:

$$g\left(\theta_{ww}\right) = \frac{e}{\cos(3\pi/8)}^{-|\theta_{ww}|} \cos\left(\frac{\theta_{ww}}{2} + \frac{3\pi}{8}\right) \tag{21}$$

The parameterization as a function of the misalignment angle (Eq. (15)), where K is computed using Eq. (6), K_{LT} is computed using Eq. (18), and $g\left(\theta_{ww}\right)$ is computed using Eq. (21), is shown in Fig. 5 by the dashed lines, showing good agreement with the diagnosed eddy viscosity values from our idealized LES.

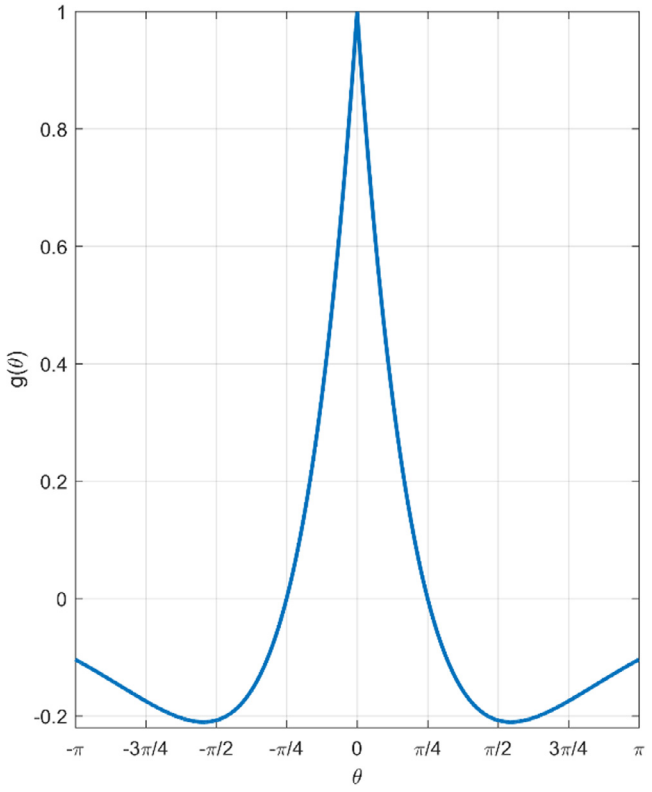

Fig. 6. Wind-wave modulation function $g(\theta_{ww})$ in range $-\pi < \theta < \pi$.

3.5. Effect of surface heat flux

In the ocean, surface heat fluxes have significant influence over the temperature distributions and the extent of the boundary layer. Global simulations show that convective turbulence dominates a significant portion (17%) of the low latitudes year-round, and about two-thirds of the world's oceans act under combined Langmuir and convective turbulence (Belcher et al., 2012; Li et al., 2019). In our simulations, buoyancy production (P_{buoy}) is enhanced in the presence of LT and became comparable with the other two production terms (Fig. 2). Furthermore, in our simulations at OWS-P the shape of the K-profiles changes significantly in the presence of LT and agreement with our parameterized eddy viscosity profiles over a wide range of surface heat fluxes (highly convective to stable) was improved by modifying the non-dimensional shape function $G(\sigma)$.

The assumptions made in the original formulation of the non-local KPP scheme are still valid when LT is present, namely zero eddy viscosity at top/bottom of the BL, zero gradient at the bottom and linear gradient at the top; the minimum degree of the polynomial needs to be 3 to accommodate for the 4 necessary constraints. Note that in the previous section we provided a scaling for the non-dimensional eddy viscosity difference at the surface, which is not zero. We use the modified Langmuir number (Eq. (16)) to provide a scaling of the overall magnitude difference of the eddy viscosity with and without LT throughout the entire BL, analogous to the suggested model in McWilliams and Sullivan (2000), which makes the eddy viscosity everywhere in the BL proportional to the turbulent Langmuir number, defined at the surface. In practice, the assumption of $G(0) = 0$ does not affect the surface scaling in ocean models, since vertical mixing variables in NCOM as well as other models such as the Regional Ocean Modeling System are defined at the grid faces and the eddy viscosity at the surface is used as the vertical boundary condition set by the wind stress. Setting $G(0) = 0$ thus offers the theoretical argument that boundary layer eddies should not cross the ocean–atmosphere interface and the practical reason that the first grid point (at the face) is not used to compute interior fluxes.

Although the minimum degree of the polynomial must be 3 to accommodate the 4 constraints, there is no reason not to increase the degree of the polynomial. By expressing the shape function $G(\sigma)$ as a binomial expansion of degree n, we can generalize and use some of its properties.

$$G(\sigma) = \sigma\,(1-\sigma)^n \tag{22}$$

$$\frac{\partial G}{\partial \sigma} = (1-\sigma)\left[1 - \frac{n\sigma}{1-\sigma}\right] \tag{23}$$

Eqs. (21) and (22) express the non-dimensional shape function and its derivative respectively, as a function of the non-dimensional coordinate σ and the expansion coefficient n, which equals 2 for simulations without LT. Fig. 7 shows the non-dimensional shape function $G(\sigma)$ (Eq. (21)) as a function of the expansion coefficient (n). By increasing the degree of the binomial expansion, we can control the magnitude and shape of the K-profiles. As a matter of fact, the maximum of G is only a function of the degree of the expansion and is found at $\max(G) = \frac{1}{n+1}$. Therefore, we assume the expansion coefficient n varies linearly with a yet undetermined dimensionless buoyancy flux parameter $\Pi_2 = f(B_0)$:

$$n = c_4 \Pi_2 + c_5 \tag{24}$$

Where (c_4, c_5) are the empirical constants used to tune our parameterization to the observed LES profiles. In the KPP, the eddy viscosity profile has a convex shape with magnitude $\sim u_*^2/f$ and a depth scale $\sim u_*/f$ (McWilliams and Huckle, 2006). Since the non-dimensional shape function sets the depth at which the eddy viscosity is maximum (Fig. 7), and the wavy Ekman layer is modified in the presence of LT (McWilliams et al., 1997, 2012), we let our dimensionless parameter Π_2 be a function of the Coriolis frequency (f). We chose the Coriolis frequency to form Π_2 because in the ocean the MLD is clearly a function of latitude, and most importantly because it is linearly independent from all other physical parameters considered and hence required by the Buckingham Pi theorem to complete the parameterization.

Since the stable stratification at the base of the mixed layer also affects the depth scale of penetration, we let our dimensionless parameter Π_2 be a function of the MLD h_m. Therefore, we normalize the surface buoyancy flux as:

$$\Pi_2 = \frac{B_0 f^3}{h_m} \tag{25}$$

Therefore, in our model the enhancement of the eddy viscosity in the presence of LT is a function of the wind stress (u_*), surface buoyancy flux (B_0), surface Stokes shear (S_0), Coriolis frequency (f), stratification (h_m), boundary layer depth (h) and wind–wave angle of misalignment (θ_{ww}). The modified shape function is given by combining Eq. (21), (23) and (24):

$$G(\sigma, \Pi_2) = \sigma\,(1-\sigma)^{c_4\Pi_2 + c_5} \tag{26}$$

3.6. LT model

In this section, we introduce our model for the enhancement of eddy viscosity in the presence of LT. We use previous suggestions by McWilliams and Sullivan (2000) and Smyth et al. (2002), but instead of parameterizing the eddy viscosity as in Eq. (18), we parameterize the eddy viscosity difference using:

$$\Delta K = h w_x(\sigma)\,\varepsilon(\Pi_1) G\left(\sigma, \Pi_2\right) g(\theta_{ww}) \tag{27}$$

Where h is the BLD computed using Eqs. (9) and (11), $G(\sigma, \Pi_2)$ is our modified shape function (Eq. (26)), $g(\theta_{ww})$ is our wind–wave modulation function (Eq. (21)) and $\varepsilon(\Pi_1)$ is the enhancement of the magnitude due to the Stokes drift, given by:

$$\varepsilon\left(\Pi_1\right) = \left(\frac{C_w}{\Pi_1^2}\right)^{\frac{1}{2}} \tag{28}$$

Table 1
Parameters and constants used in the simulations.

	Description	Nondimensional parameters	Constants	Assumptions
$\varepsilon(\Pi_1)$	Enhancement due to LT $\varepsilon(\Pi_1)$	$\left(\frac{C_w}{\left(\frac{u_*}{S_0 h_m}\right)^2}\right)^{\frac{1}{2}}$		Aligned wind–waves
$g(\theta_{ww})$	Wind-wave misalignment $g(\theta_{ww})$	$c_1 e^{-\lvert\theta_{ww}\rvert}\cos(c_2\theta_{ww}+c_3)$	$c_1 = \frac{e}{\cos(3\pi/8)}$ $c_2 = 0.5$ $c_3 = 3\pi/8$	$0 \le \theta_{ww} \le \pi$ $g(\theta_{ww}) = -g(\theta_{ww})$ $g(0) = 1; g_{min} < 0$
$G(\sigma, \Pi_2)$	Modified shape function $G(\sigma, \Pi_2)$	$\sigma(1-\sigma)^{c_4\Pi_2+c_5}$	$c_4 = 1/15$ $c_5 = 5$	Interior matching of eddy viscosity

Note that the KPP scheme from Large et al. (1994) implicitly includes the effect of LT by tuning their model constants to ocean observations, but it may misrepresent the entrainment under varying wave conditions and result in biases in boundary layer depth (Li and Fox-Kemper, 2017) and therefore the difference (Eq. (27)) reflects the correction to the original KPP scheme on the LT effect instead of the pure LT effect. The enhancements due to LT, nondimensional parameters, constants used in our parameterization are summarized in Table 1. Note that the enhancement (Eq. (27)) has a similar form to the suggested enhancement by Smyth et al. (2002), where the dominant wave direction is assumed to be aligned with the local wind direction, but scales with $La_m = \frac{u_*}{S_0 h_m}$ instead of $La_t = \frac{u_*}{U_s}$, and further drop the "plus one" since in the absence of Stokes drift there should be no enhancement (i.e., $\varepsilon(\Pi_1) \to 0$ as $\Pi_1 \to \infty$). The enhancement due to LT (Eq. (28)) is based on the formulation first suggested by McWilliams and Sullivan (2001), where the dominant wave direction is aligned with the local wind direction, but scales with $La_m = \frac{u_*}{S_0 h_m}$ instead of $La_t = \frac{u_*}{U_s}$. Similar to the surface-layer averaged Langmuir number (Harcourt and D'Asaro, 2008) we find that La_m scales well with different penetration depths, and has similar performance to the traditional turbulent Langmuir number under the idealized assumptions of aligned wind–waves and monochromatic waves. The wind–wave misalignment is modeled explicitly using Eq. (21) ($g(\theta_{ww})$), where the wind varies from 0 to 180 degrees and we assume symmetry along the aligned wind–wave direction (Fig. 6). This modification is based on a set of LES simulations under stationary wind-stress and weakly convective heat flux that show the eddy viscosity difference between simulations with and without LT is (Fig. 5) 1) maximum for aligned wind waves, no enhancement at $\theta_{ww} \sim 45°$ and minimum at $\theta_{ww} \sim 90°$, which lead to the constants used in our simulations (Table 1).

Finally, the modified shape function adjusts the local eddy viscosities, including the depth at which vertical mixing is maximum, based on the nondimensional parameter $\frac{B_0 f^3}{h_m}$. In our simulations at OWS-P, this parameter is a strong function of the surface buoyancy flux (B_0), which has significant influence on the shape of the eddy viscosities computed from LES, and we adjust the constants in NCOM to match the LES profiles. These enhancements and nondimensional parameters are discussed further in the following section.

For clarity, the complete parameterization that includes the effect of wind, waves and convection is given by:

$$K(\sigma) = h w_m(\sigma) G(\sigma) + \Delta K \tag{29}$$

Where the first term on the right is the parameterization of Large et al. (1994) and ΔK is described in Eq. (27).

4. Results

The K-Profile Parameterization as described in Large et al. (1994) was implemented in NCOM for the first time, and therefore we start by validating these results with observations and LES experiments at OWS-P. In Section 4.1 the NCOM experiment set-up is described and we briefly summarize the implementation of the SMC models. In Sections 4.2 and 4.3 we discuss the results from the simulations without and with LT, respectively, focusing on the eddy viscosity profiles. In Section 4.4 we compare all NCOM results with LES and observed temperature. Section 5 summarizes the overall performance of the schemes and further offer an intermodal comparison with other KPP models.

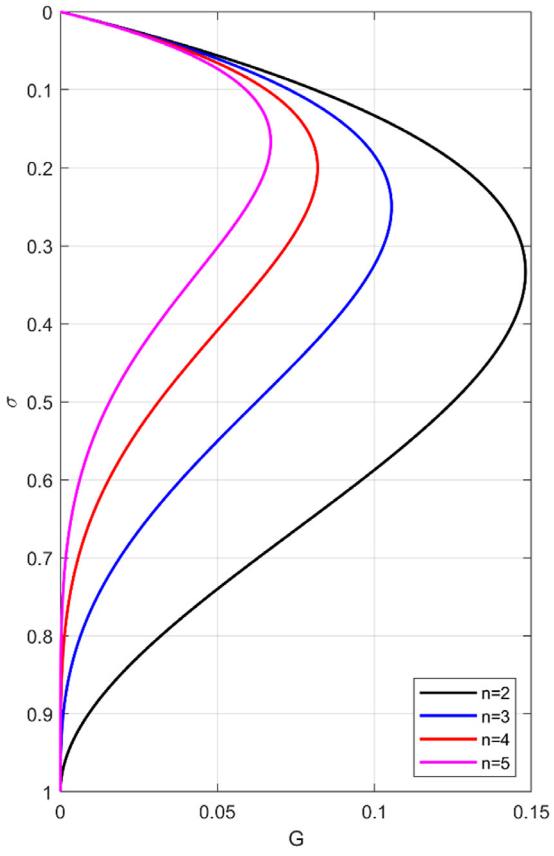

Fig. 7. Generalized shape function $G(\sigma) = \sigma(1-\sigma)^n$ with different degrees (n).

4.1. NCOM experiments

A set of 1-dimensional NCOM simulations is performed at OWS-P under the same surface forcing conditions as in the LES experiments (Fig. 1). The vertical grid uses the same number of grid points (N = 128) as the LES with similar stretching towards the surface and double periodic boundary conditions are used in the horizontal direction following the horizontal homogeneity approximation made in this study. As reported in other studies (Van Roekel et al., 2018; Li et al., 2019) we find significant sensitivity in our NCOM experiments with different vertical grid resolutions. We performed simulations with 50, 100, 128 and 150 grid points spanning the top 200 m of the ocean and show only those for 128 grid points because the difference to those with 150 grid

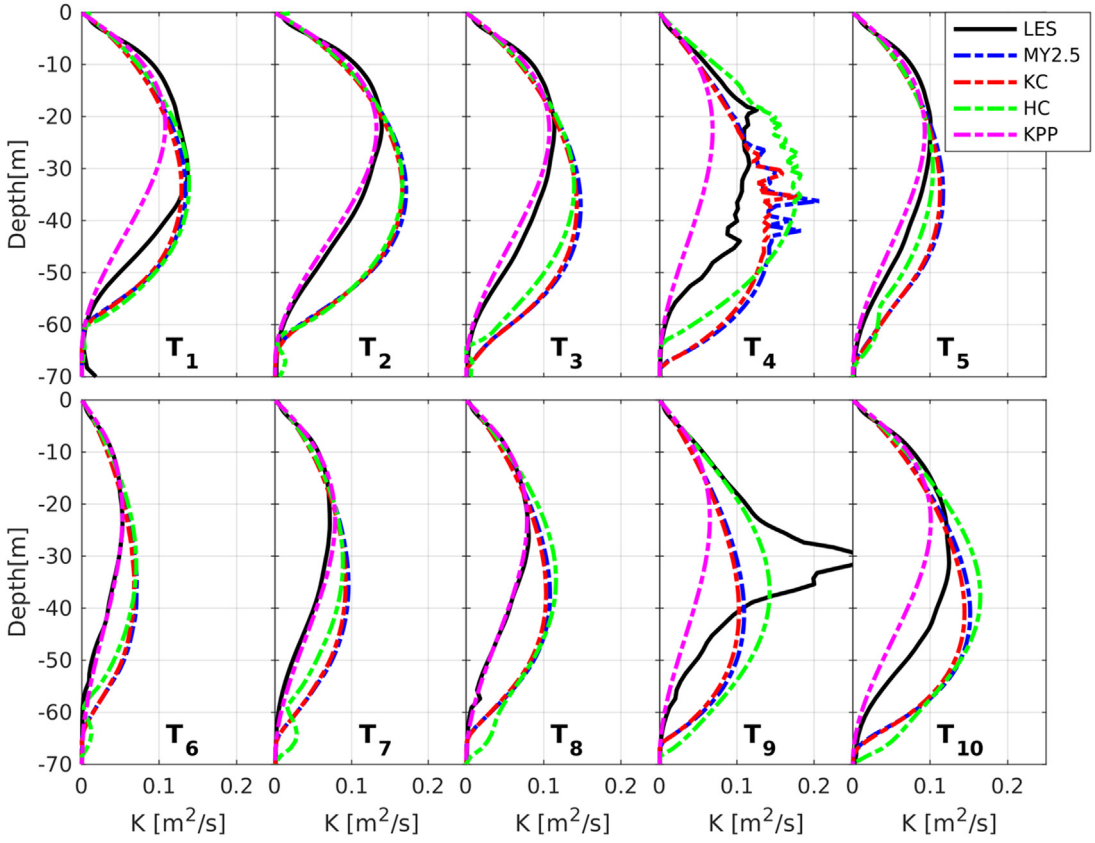

Fig. 8. Inertially averaged eddy viscosity profiles estimated from LES (black line), and NCOM simulations (dashed lines) without the effect of LT. NCOM simulations include Mellor–Yamada 2.5 (blue), Kantha–Clayson (red), Harcourt (green) and KPP (magenta).

points shows negligible difference but allows a more direct comparison with LES simulations using the same vertical resolution.

The mean velocity is initialized from rest, and temperature/salinity fields are interpolated from observations to the NCOM grid. The same procedure is followed to interpolate the Stokes drift velocity. Following the LES experiments, we assume horizontal homogeneity and use double periodic boundary conditions in the horizontal directions. Comparison of temperature profiles between observations and LES shown in Figs. 11 and 13 suggests that this is a good approximation for most of the 20 day period at OWS-P, with SST deviating from LES result only in the last 4 days.

Following the nomenclature used for the LES experiments, simulations with the effect of LT will be indicated by the "LT" label. For example, NCOM simulations using the Kantha–Clayson scheme will be labeled KC and KC-LT for simulations without and with the effect of LT, respectively. The model of Li and Fox-Kemper (2017) is labeled KPP-LF, to differentiate from out KPP-LT model.

4.2. Simulations under shear and convection only

The first set of simulations compares the vertical mixing schemes of Mellor–Yamada 2.5 (Mellor and Yamada, 1982; Kantha and Clayson, 1994; Harcourt, 2013, 2015) and KPP (Large et al., 1994), where the Stokes drift is identically zero (i.e., no LT). The implementation of these schemes is based on the original work by the authors, including the constants used to tune the contribution from shear/buoyancy production, dissipation, diffusion and transport of turbulent energy. These are also based on simulations at OWS-P for at least one year (not shown), to make sure that mixed layer deepening and restratification are accurate over long periods.

In NCOM, both KPP and SMC models use the eddy viscosity to estimate the vertical turbulent fluxes and thus provide a quantitative measure of the approximate mixing "strength" between different schemes. The inertially averaged eddy viscosities from the experiments without LT are shown in Fig. 8, where the solid black lines are from LES and the colored dashed lines are from NCOM simulations. The 10 inertial periods are taken over a 6.5 day period shown by the dashed black lines in Fig. 1, characterized by strong winds and convection (e.g. period T2), short periods of moderately misaligned wind–wave angles (periods T4, T6 and T7) and periods of moderate winds and weakly convective/neutral surface heating (periods T8-T10). For most periods the KPP scheme shows more resemblance to the diagnosed eddy viscosity from LES compared to the other SMC schemes, which on average have a higher magnitude located lower in the ML.

Results from temperature distributions is further discussed in Section 4.4.

4.3. NCOM with LT

A second set of NCOM simulations was performed to compare the performance of the Kantha and Clayson (2004) and Harcourt (2015) schemes with our proposed parameterization described in Section 4, labeled KPP-LT as well as the parameterization from Li and Fox-Kemper (2017), hereafter referred to as KPP-LF. The setup of the NCOM simulations is identical to simulations with only shear and convection, with the only difference being the addition of the Stokes drift.

First, we start by comparing the diagnosed eddy viscosity from LES-LT with the NCOM simulations, shown by color contours on a logarithmic scale in Fig. 9. During the period from November 16 to 17, characterized by strong shear, convection and Stokes drift, LES-LT shows mixing rates of about $1\ m^2/s$ and rapid ML deepening, in agreement with KPP-LT and KPP-LF models. The eddy viscosity from the KC-LT model seems to underestimate the mixing strength during this period of high turbulent production, which is improved in the HC-LT model suggesting that the corrections to the algebraic Reynold

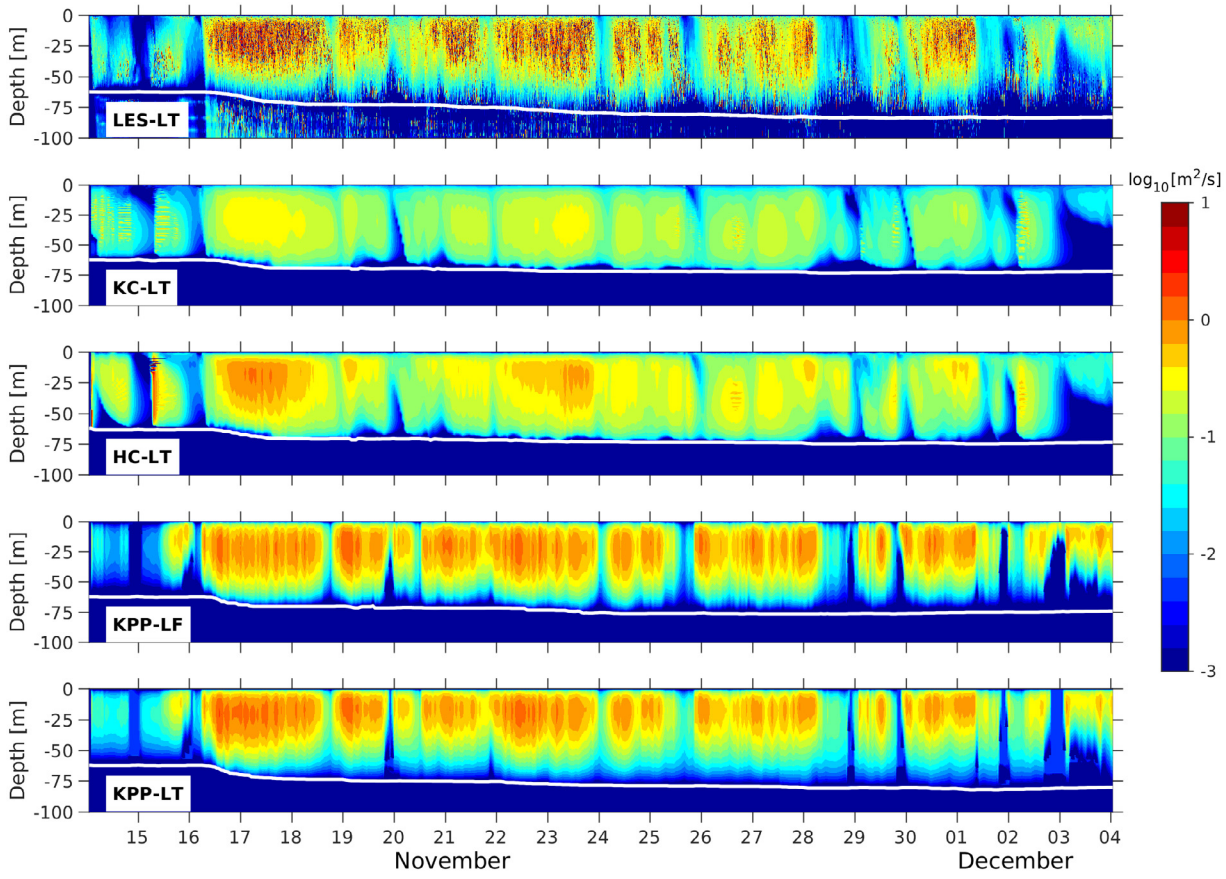

Fig. 9. Logarithmic color contours of eddy viscosity estimated in LES (top) and from NCOM simulations using Kantha–Clayson, Harcourt and KPP with the effect of LT.

stress model by Harcourt (2015) significantly improve the SMC scheme. During the last day of the simulations where surface conditions are close to neutral to weakly stable, the contours of eddy viscosity from HC-LT show good agreement, but overall both KPP-LT and KPP-LF do a reasonable job at estimating the BLD. The rapid deepening of the ML in LES-LT, indicated by the white lines in Fig. 9, is more gradual in the SMC models compared the KPP models, but all of them are underestimated compared to LES. This is discussed further in the next section.

It is hard to elucidate the differences between the KPP-LT and KPP-LF schemes from logarithmic color contours, which are more useful to compare the order of magnitude rather than precise values. Therefore, we compare the inertially averaged profiles during the period from November 16 to 23 in Fig. 10. In agreement with Fig. 9, the overall magnitude of the KPP models is larger compared to SMC schemes and in better agreement with LES. The shape of the KPP-LT model is in better agreement with LES-LT, as can be expected since we tuned our model to these results, and is of course absent from KPP-LF. During periods of wind–wave misalignment > 20° (periods T4 and T7), both the shape and magnitude of the profiles show good agreement. Under the conditions at OWS-P, that is a well-defined mixed layer and in the absence of horizontal currents (1D simulations), the improvement in KPP-LF and KPP-LT is mainly through the modification of entrainment via the turbulent velocity scale (Eq. (10)) and should be considered when parameterizing other unresolved phenomena.

4.4. Temperature

Further validation of our model is shown by comparing SST from NCOM with LES and observations presented in Fig. 11, which in the absence of horizontal gradients and under the same surface conditions closely resembles the behavior and magnitude of the MLD (not shown). For simulations under only shear and convective turbulence (top panel), the SST from MY2.5 and KC are identical, as are the result from HC and KPP models, with the latter showing slightly lower temperatures and therefore slightly greater entrainment. During the period of rapid ML deepening, SST from LES is about 0.1 degrees higher than observed which can be attributed to LT when observing that LES-LT simulations show near perfect agreement during this 2-day period. However, during the last 2 days of the simulation SST from LES-LT diverges from observations, this is most likely due to the lack of rainfall data in the simulations when heavy rainfall events were noted during these days. In the bottom panel of Fig. 11, we see that SST for our KPP-LT model is in better agreement with observations and is improved from KPP-LF by roughly 0.1 degrees, but mixing is still underestimated compared to LES and observations. This discrepancy might be explained by the lack on non-local transport in our model, since divergence from LES and observations happens during the period of strongest convection around November 17, where strong counter-gradient fluxes present in LES can play an important role in deepening the ML (Large et al., 2019b).

Fig. 12 shows color contours of the diagnosed eddy viscosity from LES with LT, superimposed with the BLD computed in three different ways: (1) using the parameterization of Large et al. (1994), (2) using Lagrangian velocities in the bulk Richardson number ($V = \sqrt{u^2 + u_S^2}$), and (3) using the surface layer averaged Langmuir number parameterization from Li and Fox-Kemper (2017). During the period of strong convection/winds around November 17, the parameterization from Large et al. (1994) becomes shallower due to the decrease of the vertical velocity gradients. While using the Lagrangian velocities (mean + Stokes) improves the estimate of the BLD during convective periods, it is still too shallow when the surface becomes stabilizing, as seen around December 1st in Fig. 12. Therefore, we find in our simulations that the parameterization of Li and Fox-Kemper (2017) for the BLD

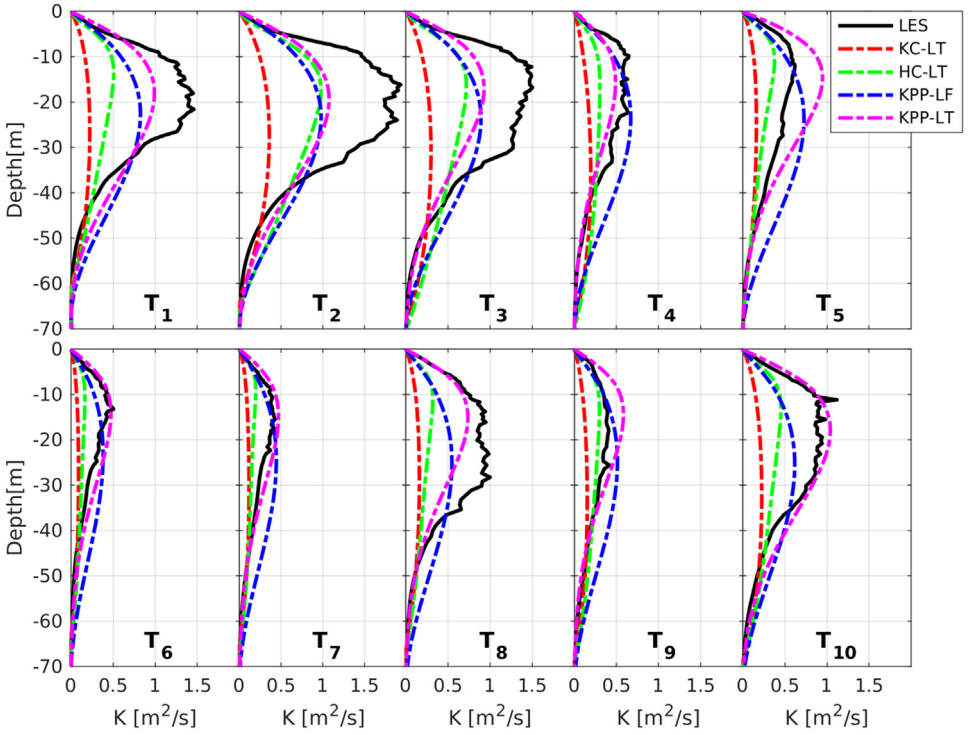

Fig. 10. Inertially averaged eddy viscosity profiles estimated from LES (black line), and NCOM simulations (dashed lines) with the effect of LT. NCOM simulations include Kantha–Clayson (red), Harcourt (green), KPP-LF (blue), and KPP_LT (magenta).

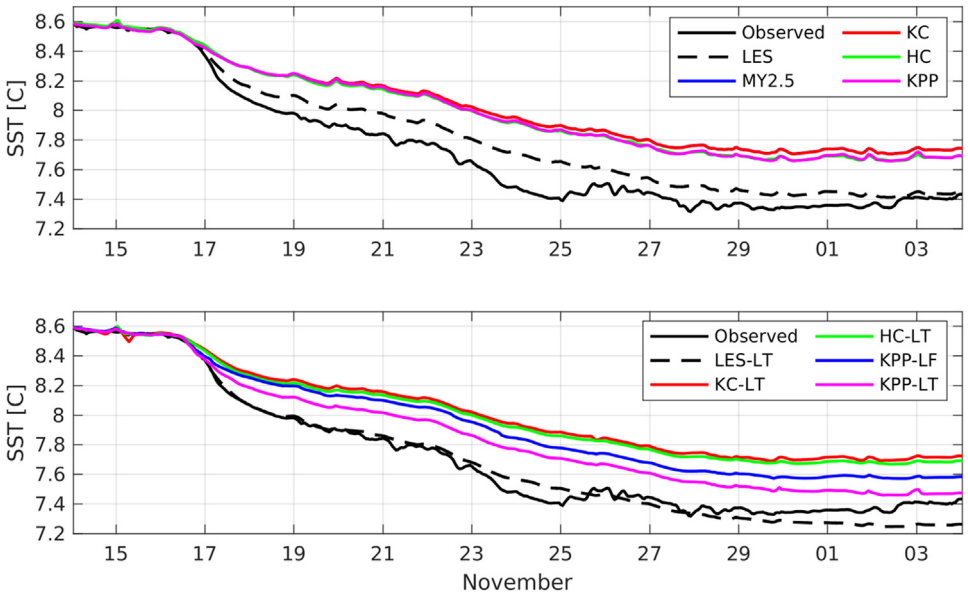

Fig. 11. SST from simulations without LT (top) and with LT (bottom). Observations are shown by the solid black line, LES by the dashed black line, and the NCOM experiments are shown by the colored lines in the legend.

to be more accurate than other suggested estimates. This also suggests that in the absence of horizontal advection it is the eddy viscosity at the pycnocline that largely influences SST and MLD, while the eddy viscosity within the mixed layer is less important.

Finally, we compare the temperature distribution in the vertical direction from our NCOM-LT simulations with LES-LT and observations in Fig. 13 for the 6.5 day period shown in Fig. 1. The solid black line in the left panel shows the observed temperature on November 16 at 7UTC when the ML is approximately 60 m deep, and the purple dots indicate the observations on November 22 at 19UTC. During this 6.5 day period the SST decreases by 1 degree, from 8.6 to 7.6 °C, and the ML deepens by almost 20 m. The LES-LT experiment (dashed purple line) shows great agreement with observations, both above and below the mixed layer with the largest error at 150 m depth and an error of less than 0.1 °C at the surface. Due to the large temperature gradient at the pycnocline, the error in temperature at 80 m depth is large for all NCOM simulations (~1 degree), but this error is significantly reduced in the KPP-LT model as well as the error with observed MLD, which is about 5 m deeper in our KPP-LT model compared to KPP-LF and SMC models. The largest differences between the LES and KPP-LT model are found below the mixed layer, where we have not modified the original formulation from Large et al. (1994) and therefore does not account

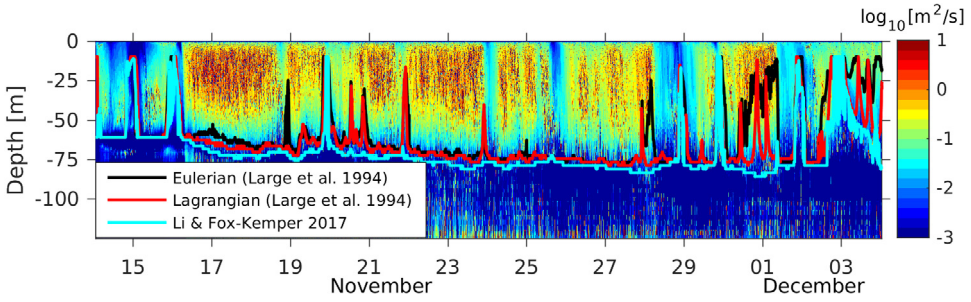

Fig. 12. Logarithmic contours of eddy viscosity ($\log_{10} K_{LT}$) from LES with LT, superimposed with boundary layer depth (h) computed using the bulk Richardson number (black line), a Lagrangian bulk Richardson number (red line) and LT parameterization by (Li and Fox-Kemper, 2017; cyan line).

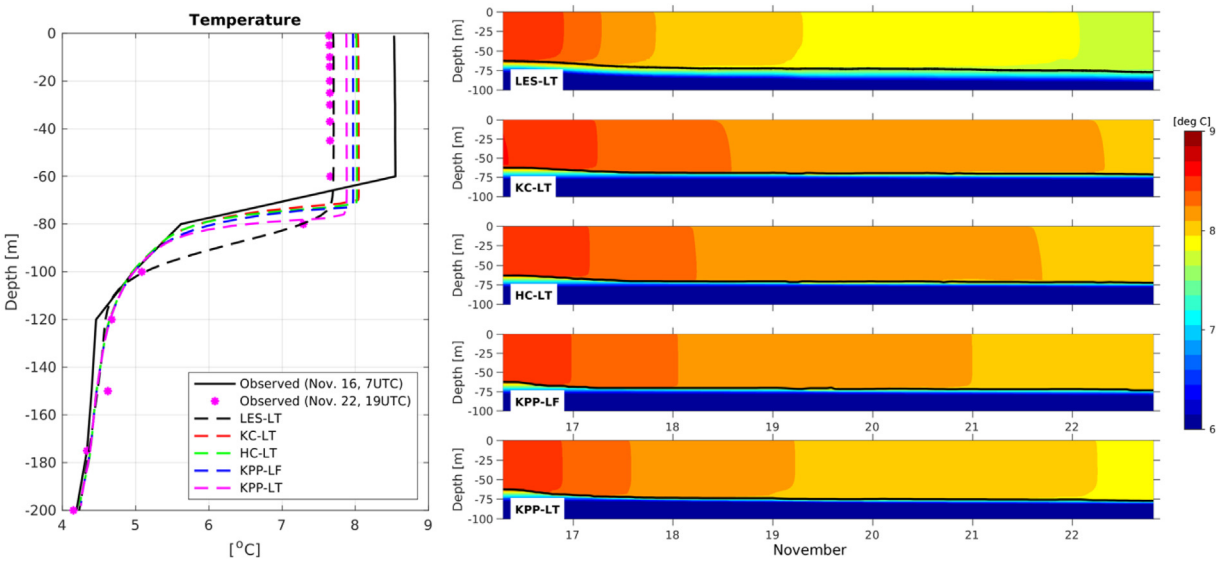

Fig. 13. (left) Observed temperature profiles at the start of the sampled period (black line), end of the period (magenta markers) and from simulations (see legend). (right) Color contours of modeled temperatures from LES and NCOM, for experiments with LT.

for other important effects in the ocean interior, such as the presence of internal waves which may potentially alter the mixed layer significantly (Garrett and Kunze, 2007). Below the BLD, the main source of vertical mixing in the KPP scheme for our simulations are shear instabilities, modeled using the gradient Richardson number (Eqs. (27) and (28) in Large et al. (1994)).

5. Summary and conclusions

A new K-profile parameterization (KPP-LT) for the enhancement of the eddy viscosity in the presence of Langmuir turbulence has been developed and implemented in the Navy Coastal Ocean Model. This model was developed and tuned using a set of LES at Ocean Weather Station Papa, spanning a 20-day period from November 14th to December 4th, 2011. LES and NCOM simulations are forced at the surface with wind stress and heat fluxes derived from observed atmospheric measurements, and the Stokes drift is computed from observed 2D wave spectra to allow the Stokes drift to evolve independently from the wind forcing (Fig. 1). In agreement with previous studies, LES at OWS-P show enhanced vertical mixing (Figs. 9 and 10) and TKE (Fig. 2) in the presence of LT, significant reduction of shear production by the mean currents (P_{shear}) with enhanced vertical transport, Stokes production (P_{Stokes}) and buoyancy production (P_{buoy}) resulting in a deeper mixed layer depth and in the absence of lateral horizontal gradients, lower SST with better agreement with observations.

A set of idealized LES experiments under different wind–wave angles of misalignment (θ_{ww}) was used to parameterize the effect of the misalignment between the wind stress and Stokes drift. These simulations show that the vertical mixing is maximum for the case of aligned wind–wave angles (i.e., $\theta_{ww} = 0$), but further increasing this angle leads to no enhancement ($\theta_{ww} \sim 45 \rightarrow 60°$) over simulations without LT and even reduction in the turbulent energy (Figs. 2 and 7) for very high wind–wave angles ($\theta_{ww} > 60$).

The KPP-LT scheme (Eq. (22)) is based on the non-local KPP scheme (Large et al., 1994), with 4 important modifications: (1) increased entrainment of buoyancy flux parameterized via the bulk Richardson number (Li and Fox-Kemper, 2017), (2) the enhancement of vertical mixing by LT ($\varepsilon(\Pi_1)$) based on suggestions by McWilliams and Sullivan (2000) and Smyth et al. (2002), (3) the effect of the surface buoyancy flux through modifications to the non-dimensional shape function $G(\sigma, \Pi_2)$, and (4) the wind–wave angle of misalignment through the wind–wave modulation function $g(\theta_{ww})$. In our model, the enhancement due to the inclusion of the Stokes drift is parameterized using a modified Langmuir number ($\Pi_1 = La_m$), which shows better scaling with our non-dimensional eddy viscosity (Π, Eq. (13)). Our NCOM experiments show improvement of the eddy viscosity in KPP simulations compared to SMC models, both with and without the effect of LT (Figs. 8 and 10).

An important goal of this paper was to highlight the advantages and limitations of current SMC and KPP models, which still show significant differences under the same forcing conditions in ocean simulations. By far the largest shortcoming of the KPP model, as presented in this study and conceptualized by Large et al. (1994), is the assumption of an immobile surface which makes it complicated to represent the ocean's surface dynamics, which is formally addressed in Large et al. (2019a,b). SMC models have addressed the need for additional turbulence due to

Stokes drift by injecting additional TKE at the surface, using the dot product of wind stress and Stokes drift as a scaling parameter (Kantha et al., 2010) that considers wind–wave misalignment. Finally, in this study we do not address the issue of nonlocal transport that has been shown to be important in highly convective flows or the role of vertical grid resolution in the accuracy of SMC and KPP models. In view of these limitations, it seems necessary that new parameterizations are proposed that prioritize these issues to start with, since they have proved to be highly elusive.

Declaration of competing interest

The authors declare that they have no known competing financial interests or personal relationships that could have appeared to influence the work reported in this paper.

Acknowledgments

We would like to express our appreciation to the anonymous reviewers for their constructive comments. Computations for this study were performed at the Navy DoD Supercomputing Resource Center (DSRC). The research was funded by the Office of Naval Research under program element 062435N. This paper is a contribution of NRL/JA/7320-20-4996, and has been approved for public release.

Appendix. The subgrid scale (SGS) model

The SGS model in the NCAR LES model was originally developed by Moeng (1984). The prognostic equation for the subgrid scale (SGS) turbulent kinetic energy (TKE) e' is given as:

$$\frac{\partial e'}{\partial t} + \vec{u} \cdot \nabla e' = P' + B' + D' - \varepsilon' \tag{A.1}$$

where $\vec{u}$ is the resolved velocity vector, the terms on the right side are subgrid-scale production (P'), buoyancy (B'), diffusion (D'), and dissipation ε':

$$P' = -\tau'_{ij} S_{ij} \tag{A.2}$$

with the strain tensor: $S_{ij} = \frac{1}{2}\left(\frac{\partial u_i}{\partial x_j} + \frac{\partial u_j}{\partial x_i}\right)$ and the SGS momentum flux (stress): $\tau'_{ij} = -2\nu_t S_{ij}$

$$B' = -\nu_\theta \frac{g}{\theta_0} \frac{\partial \theta}{\partial x_i} \tag{A.3}$$

$$D' = \frac{\partial}{\partial x_i}\left(2\nu_t \frac{\partial e}{\partial x_i}\right) \tag{A.4}$$

$$\varepsilon' = \frac{C e^{3/2}}{l} \tag{A.5}$$

In the above equations, θ is heat, ν_t is the SGS turbulent eddy viscosity, ν_θ is the SGS eddy diffusivity for scaler, and C and l are the Smagorinsky constant and length scale.

Sullivan et al. (2007) further improved this model to include the effect of Stokes production and wave breaking by adding three new terms to the right side of (A.1):

$$-u_j^{st} \frac{\partial e}{\partial x_j} - \tau'_{ij} \frac{\partial u_i^{st}}{\partial x_j} + \sum_m W^m$$

where the superscript st represents Stokes drift, and the effects of $m = 1, \ldots, M$ discrete wave-breaking events are represented by a subgrid-scale TKE generation rate W^m. Since wave breaking is not considered in this study, W^m is set to zero for all experiments.

References

Belcher, S., Grant, A., Hanley, K., Fox-Kemper, B., Van Roekel, L., Sullivan, P., et al., 2012. A global perspective on Langmuir turbulence in the ocean surface boundary layer. Geophys. Res. Lett. 39, 1–9.

Craik, A., Leibovich, S., 1976. A rational model for langmuir circulations. J. Fluid Mech. 73, 401–426.

D'Asaro, E., 2001. Turbulent vertical kinetic energy in the ocean mixed layer. J. Phys. Oceanogr. 31, 3530–3538.

de Boyer Montegút, C., Madec, G., Fischer, A.S., Lazar, A., Iudicone, D., 2004. Mixed layer depth over the global ocean: An examination of profile data and a profile-based climatology. J. Geophys. Res. 109, C12003. http://dx.doi.org/10.1029/2004JC002378.

Fairall, C.W., Bradley, E.F., Hare, J.E., Grachev, A.A., Edson, J.B., 2003. Bulk parameterization of air–sea fluxes: Updates and verification for the COARE algorithm. J. Clim. 16, 571–591.

Fan, Y., Yu, Z., Savelyev, I., Sullivan, P., Liang, J., Haack, T., Eric, T., Paolo, T., Shearman, K., 2020. The effect of Langmuir turbulence under complex real oceanic and meteorological forcing. Ocean Model. 149, 1463–5003. http://dx.doi.org/10.1016/j.ocemod.2020.101601.

Gargett, A., Wells, J., Tejada-Martinez, A., Grosch, C.E., 2004. Langmuir supercells: a mechanism for sediment resuspension and transport in shallow seas. Science 306, 1925–1928.

Garrett, C., Kunze, E., 2007. Internal tide generation in the Deep Ocean. Annu. Rev. Fluid Mech. 39, 57–87. http://dx.doi.org/10.1146/annurev.fluid.39.050905.110227.

Grant, A., Belcher, S., 2009. Characteristics of Langmuir turbulence in the ocean mixed layer. J. Phys. Oceanogr. 39, 1871–1887.

Hanely, K., Belcher, S., Sullivan, P., 2010. A global climatology of wind-wave interaction. J. Phys. Oceanogr. 40, 1263–1282.

Haney, S., 2015. Symmetric and geostrophic instabilities in the wave-forced ocean mixed layer. J. Phys. Oceanogr. 45, 3033–3056.

Harcourt, R., 2013. A second-moment closure model of Langmuir turbulence. J. Phys. Oceanogr. 43, 673–697.

Harcourt, R., 2015. An improved second-moment closure model of Langmuir turbulence. J. Phys. Oceanogr. 45, 84–103.

Harcourt, R., D'Asaro, E., 2008. Large-eddy simulation of Langmuir turbulence in pure wind seas. J. Phys. Oceanogr. 38, 1, 542-1, 562.

Kantha, L., Clayson, C.A., 1994. An improved mixed layer model for geophysical application. J. Geophys. Res. 99 (C12), 25, 235-25, 266.

Kantha, L., Clayson, C.A., 2004. On the effect of surface gravity waves on mixing in the oceanic mixed layer. Ocean Model. 6, 101–124.

Kantha, Lakshmi, Lass, Hans, Prandke, Hartmut, 2010. A note on Stokes production of turbulence kinetic energy in the oceanic mixed layer: Observations in the Baltic Sea. Ocean Dyn. 60, 171–180. http://dx.doi.org/10.1007/s10236-009-0257-7.

Kenyon, K.E., 1969. Stokes drift for random gravity waves. J. Geophys. Res. 74 (28), 6991–6994. http://dx.doi.org/10.1029/JC074i028p06991.

Kukulka, T., Brunner, K., 2015. Passive buoyant tracers in the ocean surface boundary layer: 1. Influence of equilibrium wind-waves on vertical distributions. J. Geophys. Res. Oceans 120, 3837–3858. http://dx.doi.org/10.1002/2014JC010487.

Kukulka, T., Harcourt, R., 2017. Influence of Stokes drift decay scale on Langmuir turbulence. Phys. Oceanogr. 47, 1637–1656.

Kukulka, T., Plueddemann, A.J., Sullivan, P.P., 2013. Inhibited upper ocean restratification in nonequilibrium swell conditions. Geophys. Res. Lett. 40, 3672–3676. http://dx.doi.org/10.1002/grl.50708.

Large, W., McWilliams, J., Doney, S., 1994. Oceanic vertical mixing: a review and a model with a nonlocal boundary layer parameterization. Rev. Geophys. 32 (4), 363–403.

Large, W.G., Patton, E.G., DuVivier, A.K., Sullivan, P.P., Romero, L., 2019a. Similarity theory in the surface layer of large-eddy simulations of the wind-, wave-, and buoyancy-forced southern ocean. J. Phys. Oceanogr. 49 (8), 2165–2187.

Large, W.G., Patton, E.G., Sullivan, P.P., 2019b. Nonlocal transport and implied viscosity and diffusivity throughout the boundary layer in LES of the southern ocean with surface waves. J. Phys. Oceanogr. 49 (10), 2631–2652.

Li, Q., Fox-Kemper, B., 2017. Assessing the effects of Langmuir turbulence on the entrainment buoyancy flux in the ocean surface boundary layer. J. Phys. Oceanogr. 47, 2863–2886.

Li, M., Garrett, C., Skyllingstad, E., 2005. A regime diagram for classifying turbulent large eddies in the upper ocean. Deep Sea Res. I 52, 259–278.

Li, Q., Reichl, B.G., Fox-Kemper, B., Adcroft, A.J., Belcher, S.E., Danabasoglu, G., et al., 2019. Comparing ocean surface boundary vertical mixing schemes including Langmuir turbulence. J. Adv. Modelling Earth Syst. 11, 3454–3592. http://dx.doi.org/10.1029/2019MS001810.

McWilliams, J., Huckle, E., 2006. Ekman layer rectification. J. Phys. Oceanogr. 36, 1646–1659.

McWilliams, J., Huckle, E., Liang, J., 2014. Langmuir turbulence in swell. Phys. Oceanogr. 44, 870–890.

McWilliams, J., Huckle, E., Liang, J.-H., Sullivan, P., 2012. The wavy Ekman layer: Langmuir circulations, breaking waves, and Reynolds stress. J. Phys. Oceanogr. 42, 1, 793–1, 816.

McWilliams, J., Sullivan, P., 2000. Vertical mixing by Langmuir circulations. Spill Sci. Technol. Bull. 6, 225–237.
McWilliams, J., Sullivan, P., 2001. Surface-Wave Effects on Winds and Currents in Marine Boundary Layers. Fluid Mech. Environ.: Dyn. Approaches 201–224.
McWilliams, J., Sullivan, P., Moeng, C.-h., 1997. Langmuir turbulence in the ocean. Fluid Mech. 334, 1–30.
Mellor, G., Yamada, T., 1982. Development of a turbulence closure model for geophysical applications. Rev. Geophys. 20, 851–875.
Moeng, C.-H., 1984. A large-eddy-simulation model for the study of the planetary boundary layer turbulence. J. Atmos. Sci. 41, 2052–2062.
Pearson, B., Grant, A., Polton, J., Belcher, S., 2018. Reply to Comments on 'Langmuir turbulence and surface heating in the ocean surface boundary layer'. J. Phys. Oceanogr. 48, 459–462.
Price, J., Sundermeyer, M., 1999. Stratified Ekman layers. J. Geophys. Res. Oceans 104, C9, 20, 467-20, 494.
Reichl, B., Wang, D., Hara, T., Ginis, I., Kukulka, T., 2016. Langmuir turbulence parameterization in tropical cyclone conditions. J. Phys. Oceanogr. 46, 863–886.
Skyllingstad, E., Denbo, D., 1995. An ocean large-eddy simulation of Langmuir circulations and convection in the surface mixed layer. J. Geophys. Res. 100, 8, 501–8, 522.
Smyth, W., Skyllingstad, E., Crawford, G., Wisejekera, H., 2002. Nonlocal fluxes and Stokes drift effects in the K profile parameterization. Ocean Dyn. 10, 4–115.
Sullivan, P., McWilliams, J., Melville, W., 2007. Surface gravity wave effects in the oceanic boundary layer: Large-eddy simulation with vortex force and stochastic breakers. J. Fluid Mech. 593, 405–452.
Sullivan, P., Romero, L., McWilliams, J., Melville, W., 2012. Transient evolution of Langmuir turbulence in ocean boundary layers driven by hurricane winds and waves. J. Phys. Oceanogr. 42, 1959–1980.
Sutherland, G., Christensen, K., Ward, B., 2014. Evaluating Langmuir turbulence parameterizations in the ocean surface boundary layer. J. Geophys. Res. Oceans 119, 1, 899–1, 910.
Tennekes, H., 1973. A Model for the Dynamics of the Inversion Above a Convective Boundary Layer. J. Atmos. Sci. 30 (4), 558–567.
Thomson, J., D'Asaro, E.A., Cronin, M.F., Rogers, W.E., Harcourt, R.R., Shcherbina, A., 2013. Waves and the equilibrium range at Ocean Weather Station P. J. Geophys. Res. Oceans 118, 5951–5962. http://dx.doi.org/10.1002/2013JC008837.
Troen, I.B., Mahrt, L., 1986. A simple model of the atmospheric boundary layer; sensitivity to surface evaporation. Bound.-Layer Meteorol. 37, 129–148. http://dx.doi.org/10.1007/BF00122760.
Umlauf, L., Burchard, H., 2003. A generic length scale equation for geophysical turbulence models. J. Mar. Res. 61, 235–265.
Van Roekel, L.P., Adcroft, A., Danabasoglu, G., Griffies, S.M., Kauffman, B., Large, W.G., et al., 2018. The KPP boundary layer scheme for the ocean: Revisiting its formulation and benchmarking one-dimensional simulations relative to LES. J. Adv. Modelling Earth Syst. 10, 2647–2685. http://dx.doi.org/10.1029/2018MS001336.
Van Roekel, L., Fox-Kemper, B., Sullivan, P., Hamlington, P., Haney, S., 2012. The form and orientation of Langmuir cells for misaligned wind-waves. J. Geophys. Res. 117, 1–22.
Webb, A., Fox-Kemper, B., 2015. Impacts of wave spreading and multidirectional waves on estimating Stokes drift. Ocean Model. 96, 49–64. http://dx.doi.org/10.1016/j.ocemod.2014.12.007.
Zikanov, O., Slinn, D., Dhanak, M., 2003. Large-eddy simulations of wind-induced turbulent Ekman layer. J. Fluid Mech. 495, 343–368.